THE JOURNAL OF PHYSICAL CHEMISTRY C

Article

Cite This: J. Phys. Chem. C 2019, 123, 5907−5922

pubs.acs.org/JPCC

Charge-Transport Mechanisms in Azurin-Based Monolayer Junctions

Published as part of The Journal of Physical Chemistry virtual special issue "Abraham Nitzan Festschrift".

Stephanie Valianti,[†] Juan-Carlos Cuevas,[‡] and Spiros S. Skourtis*[,†]

[†]Department of Physics, University of Cyprus, 1678 Nicosia, Cyprus

[‡]Departamento de Física Teórica de la Materia Condensada and Condensed Matter Physics Center (IFIMAC), Universidad Autónoma de Madrid, E-28049 Madrid, Spain

Supporting Information

ABSTRACT: We study the transport mechanisms of different types of azurin (Az) monolayer heterojunctions with a variety of metal substituents. The systems include Holo-Az (Cu-substituted), Apo-Az (no metal), and Ni-, Co- and Zn-substituted azurins. Our theoretical analysis is based on measurements of the voltage and temperature dependencies of the current and attempts to reproduce both dependencies using a common mechanism and corresponding set of parameters. Our results strongly suggest that for Holo-Az the transport mechanism depends on the protein monolayer/heterojunction setup. In one type of heterojunction, transport is dominated by resonant incoherent hopping through the Cu redox site, whereas in the other it is mediated by off-resonant tunneling. For the unsubstituted (Apo-Az) and other metal-substituted azurins, the dominant transport mechanism at low temperatures is off-resonant tunneling, with an average tunneling barrier that depends on the type of metal dopant, and at the highest temperatures, it is through-amino-acid hopping. Our modeling results are relevant to the analysis of the current behavior over a range of temperatures for any molecular heterojunction device.

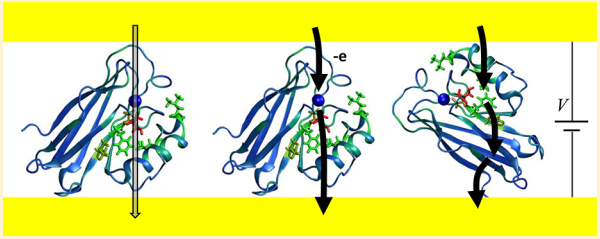

1. INTRODUCTION

Biomolecular electron-transfer (ET) reactions participate in many biological functions such as biological energy conversion processes, biological signaling pathways, and disease-repair mechanisms.[1−10] Biomolecular ET reactions are often components of ET chains that are hopping networks of donor-to-acceptor charge-transfer rates.[3] The electron/hole donor (D) and acceptor (A) moieties in these chains are atom or molecule dopants embedded in protein or DNA matrices that act as the bridge (B) connecting donors to acceptors.[5−7] Each D-to-A hopping step of the network involves through-protein or through-DNA electron tunneling. The D-to-A electronic couplings and D-to-A activation energies of each step determine the magnitude of the corresponding D-to-A ET hopping rate (k_{ET}).[11−14] Biological ET chains can operate over a variety of length scales (from nanometer to over micrometer distances).[8,9]

Over the past decades, experimental, theoretical, and computational studies of ET molecules and ET proteins (ETpr's) have shown that it is possible to tune molecular ET rates and the charge flow in biological ET chains by chemical modifications of the donor, the acceptor, and the bridge by changing the locations of the donor and the acceptor or by modifying the solvent environment.[4,7,11−18]

ETpr's are also of interest in molecular electronics.[19,20] Because there is extensive knowledge of how to tune the solution-phase through-protein ET mechanisms by chemical modifications,[7,11] an attractive idea is to use ETpr's as the main current-carrying material in hybrid electronic devices. Chemical modifications of the ETpr's in the device may enable tuning the through-protein current and thus the functionality of the device.[21,22]

Solution-phase ET reactions mediated by blue copper proteins, (containing a Cu ion as the redox center) and, in particular, azurin, have been studied thoroughly both experimentally and computationally (e.g., refs 7, 16, 17, 23, 24 and references therein). In addition to the solution-phase ET studies, there are several experiments that measure transport (current) through azurin in different types of molecular junction setups, for example, refs 25−28 are early works.

This work focuses on two experiments[29,30] that measure the current−voltage and current−temperature characteristics of Az monolayer heterojunctions. Reference 29 (also denoted exp. I) reported current measurements for heterojunctions composed of oriented Az monolayers sandwiched between an Si-oxide substrate and a gold (Au) or mercury (Hg) macroscopic LOFO (lift-off, float-on) contact[31] with an area of 0.2 mm^2. In the present study, we focused on the experiments conducted with the Au LOFO contact for comparison purposes with the results of ref 30 (see below). The experiments in ref 29 observed temperature-independent transport across the Az

Received: January 6, 2019
Revised: February 18, 2019
Published: February 20, 2019

DOI: 10.1021/acs.jpcc.9b00135
J. Phys. Chem. C 2019, 123, 5907−5922

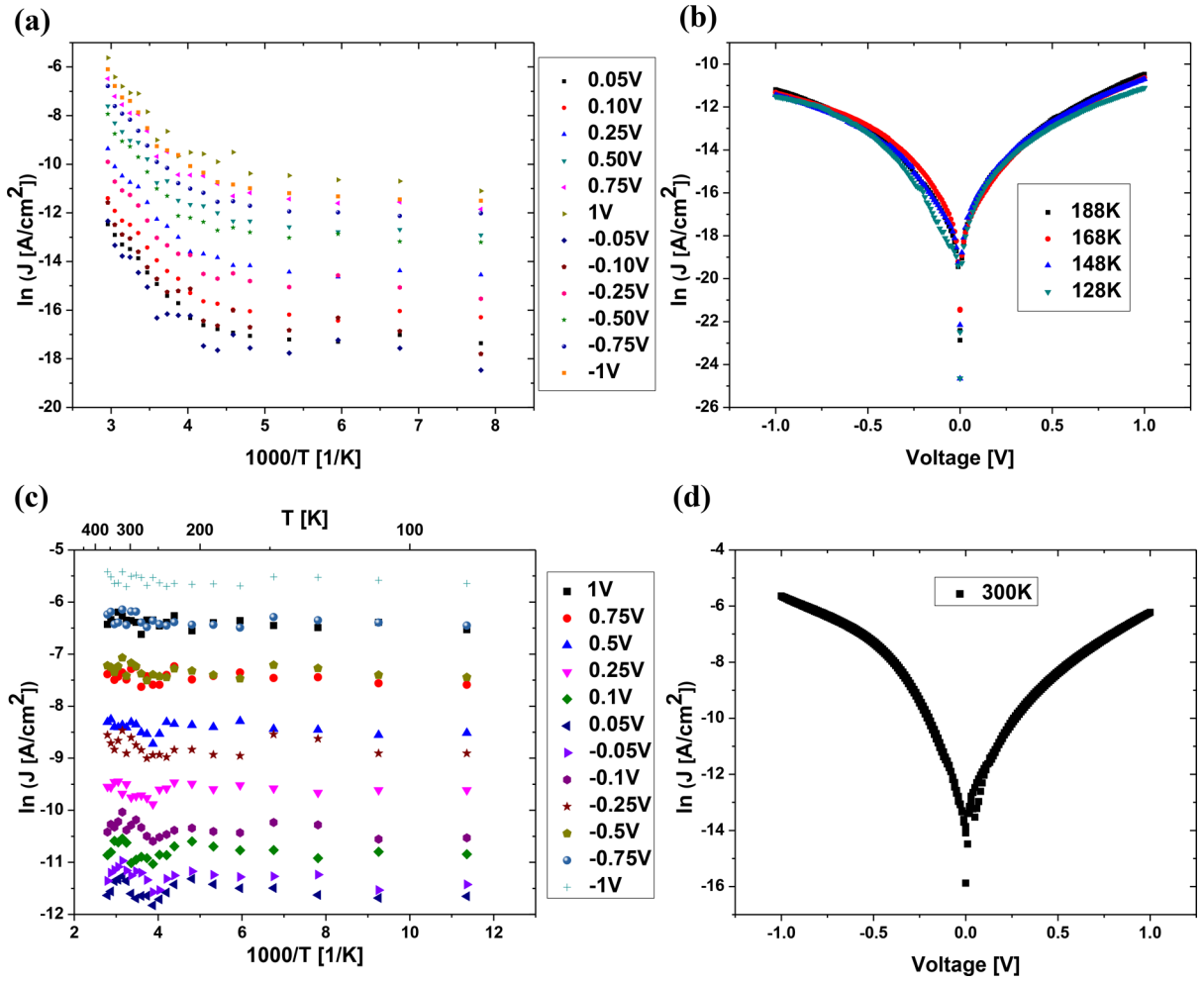

Figure 1. (a) Experimental current density (current per unit area) versus temperature (ln(J) versus 1000/T) for Apo-Az at different bias voltages. (b) Experimental ln(J) versus V for Apo-Az at T = 128, 148, 168, and 188 K. (c) Experimental ln(J) versus 1000/T of Holo-Az at different bias voltages. (d) Experimental ln(J) versus V of Holo-Az junction at room temperature[29] (exp. I).

monolayer (transport distance is ~3.5 nm) for a wide range of temperatures (T = 100−400 K) for Az molecules containing Cu (Holo-Az). When the Cu atom is removed from Az (Apo-Az), the current (I) through the monolayers is reduced by more than two orders of magnitude as compared with Holo-Az for T < 200 K. Also, for Apo-Az, the current becomes temperature-dependent for T > 200 K. We summarize the experimental results of exp. I in Figure 1.

An interesting observation in ref 29 is that substitutions of Apo-Az with metals other than Cu show temperature dependencies that are intermediate between Apo-Az and Holo-Az (see Figure 2 below).

Reference 30 (also denoted exp. II) reported experiments on oriented Holo-Az monolayers sandwiched between soft Au microelectrodes using the "suspended-wire" technique.[32,33] The currents measured in ref 30 are temperature-independent[34] for a range of temperatures from 25 to 275 K (see Figure 3).

The above-mentioned experiments involve different numbers of proteins in the monolayer ($N_{contact} \approx 10^7$ to 10^9 for ref 29 and $N_{contact} \approx 50$−200 for ref 30). Furthermore, in the first experiment,[29] the proteins in the monolayer are covalently bound to the P^{2+} Si/oxide Si substrate via the exposed cysteine residue (Cys3 or Cys26) that binds to a (~6 Å) 3-MPTMS linker molecule. The other side of the monolayer is

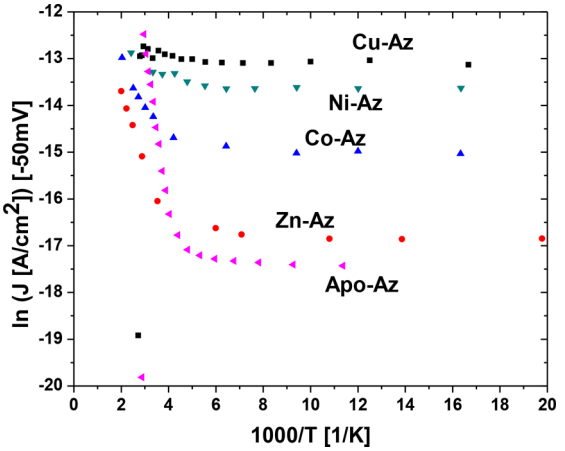

Figure 2. Experimental ln(J) versus 1000/T of Holo-, Ni-, Co-, Zn-, and Apo-Az junction at −50 mV bias[29] (exp. I).

physisorbed to the Au/Hg LOFO. In the second experiment,[30] the proteins in the monolayer are covalently bound to both Au substrates by an S−Au bond between the Au and one of the relatively exposed Az cysteine thiolates.

Figure 4 is an example of the normalized current, on the linear scale, as a function of voltage for the two experi-

DOI: 10.1021/acs.jpcc.9b00135
J. Phys. Chem. C 2019, 123, 5907−5922

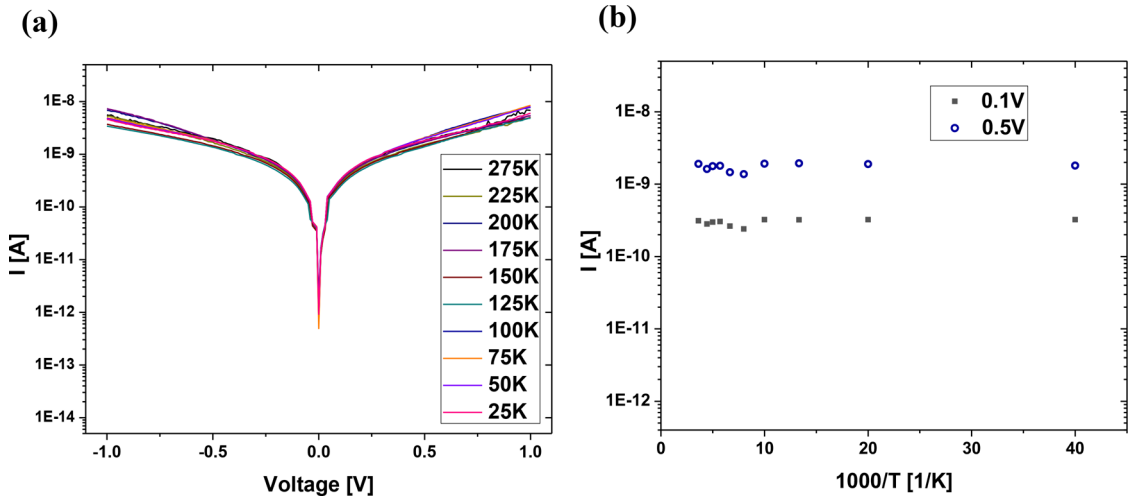

Figure 3. Experimental current−voltage curves via Holo-Az: (a) I versus V ($-1 \leq V \leq 1$), with current plotted as log(I), at different temperatures. (b) Current at 0.1 and 0.5 V, indicating the same temperature-independent behavior at different bias voltages[30] (exp. II).

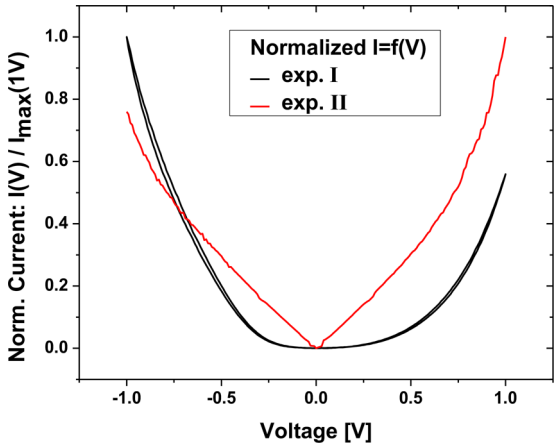

Figure 4. Comparison of current−voltage behaviors in experiments I (ref 29) and II (ref 30). Each current is normalized by its value at 1.0 V, and the temperature is 200 K.

ments.[29,30] (The normalization is with respect to the current value at 1.0 V.) Note that the normalized current in ref 29 grows slowly around $V = 0$, whereas in ref 30 it grows more rapidly and almost linearly. Comparing the two graphs (Figure 4), the I−V values have very different shapes, especially in the low voltage ($V < 0.5$ V) regime. Also, the current per molecule, $I = I_{total}/N_{contact}$, at a constant voltage value seems to be very different in the two experiments. For example, for $V = 0.1$ V and using the above-mentioned and approximate coverages, $I = 6.0 \times 10^{-19}$ to 6.0×10^{-17} A in ref 29 and $I = 1.5 \times 10^{-12}$ to 6.0×10^{-12} A in ref 30. This difference is probably due to the insulating layer added by the SiOx and a linker in the setup of ref 29, which lowers the current by some orders of magnitude, because $I \approx e^{-\beta R}$, where β is the tunneling decay parameter for Az at the average injection energy and R is the molecular bridge's length.[34] Therefore, even though the protein transport medium in both experiments is the same (Az monolayers), the transport mechanisms in the two systems seem to be different.

In the present work, we will study the I−V and I−T behaviors reported in the experiments using different phenomenological models that describe possible transport mechanisms (see below). We will also attempt to explain the changes in current behavior seen when the Cu ion is removed from Az (see Figure 1a,b). To our knowledge, there is still no comprehensive theoretical modeling of both experiments. Our modeling results are relevant to the analysis of the current behavior over a range of temperatures for any molecular heterojunction device.

2. THEORETICAL METHODS

We will present and discuss results for current−voltage and current−temperature measurements as reported in both experiments[29,30] using different basic models that relate to different transport mechanisms. These include the one-site hopping model,[13,14,20,35,36] the Landauer off-resonant tunneling and resonant tunneling models,[13,14,19] multisite extensions of these models, the extended fully adiabatic Newns−Anderson model,[37−40] and the two-step ET model (2sETm).[41,42] These models are motivated by the experiments[29,30] and are described in full detail below.

For all models, in the schematic representation (Figure 5), L(R) denotes the left (right) electrodes, where the protein

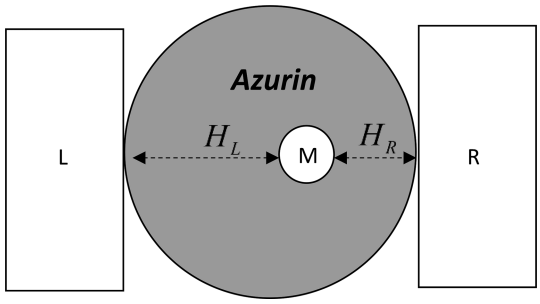

Figure 5. Schematic representation of the layout used for the description of some theoretical models to describe the experiments. M denotes metal dopant (e.g., Cu) and H_L and H_R are the protein-mediated tunneling matrix elements between L and R electrodes.

azurin and the binding ligands are placed between them. For the experimental setup of ref 29, R represents the LOFO (Au or Hg) and L represents the substrate (Si/oxide Si). It is believed that on average Cu is closer to the R electrode. However, in our modeling, we do not make any assumptions about orientation. For the experiments of ref 30, R and L represent Au electrodes.

DOI: 10.1021/acs.jpcc.9b00135
J. Phys. Chem. C 2019, 123, 5907−5922

For an Az monolayer of $N_{contact}$ molecules, the total current is approximated by $I_{total} = N_{contact}I$, and below we describe several models for I. The experiments measure a current density $J = I_{total}/A$, where A is the total contact area. It should be noted that the effective number of contacts (molecules) in these experiments is to some extent an uncertain variable due to the complexity of the heterojunctions. Also, the effective number of contacts will depend on the extent of intermolecular interactions,[43] which is also unknown. Thus, in our fitting, we probe a range of $N_{contact}$ values, and we place more importance on modeling the experimental temperature and voltage dependencies rather than the absolute current values.

The first set of models used describes coherent transport and is based on the Landauer formalism.[13,14,19] The current per molecule is given by

$$I(V) = -e\int dE\,\frac{1}{\pi\hbar}T(E,V)[f(E+eV/2) - f(E-eV/2)] \quad (1)$$

where

$$T(E,V) = \frac{4\Gamma_L\Gamma_R}{[E-\varepsilon_0(V)]^2 + [\Gamma_L+\Gamma_R]^2} \quad (2)$$

is the transmission probability, V is the voltage bias across the junction, $-eV/2 = \mu_L$ (the Fermi energy of L electrode), and $+eV/2 = \mu_R$ (the Fermi energy of R electrode) (see Figure 6).

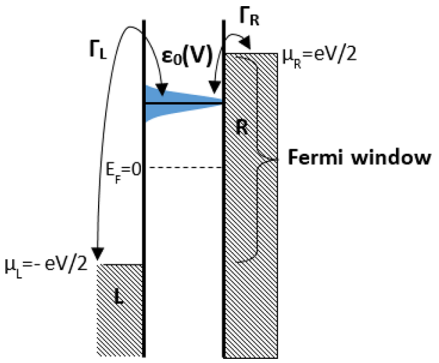

Figure 6. Schematic representation of the basic parameters used in the Landauer models (ε_0 (V), $\Gamma_{L(R)}$).

Here $\varepsilon_0(V)$ is a molecular level energy, which acts as a transmission channel

$$\varepsilon_0(V) = \varepsilon_0 + (\alpha - 1/2)\ \text{eV} \quad (3)$$

The dependence of the level energy on bias enters via a parameter α. For example, if $\alpha = 0.5$, then the level energy is independent of voltage. For $\varepsilon_0 = 0$ and $\alpha = 0$, it is pinned to μ_L, and for $\varepsilon_0 = 0$ and $\alpha = 1$, it is pinned to μ_R. Moreover, $\Gamma_{L(R)}$ are the level broadenings associated with the level couplings $H_{L(R)}$ to the L(R) leads (see Figure 5)

$$\Gamma_{L(R)} = \pi H^2_{L(R)}\rho_{L(R)} \quad (4)$$

where $\rho_{L(R)}$ are the electronic densities of states of the L(R) leads. These broadenings are related to the Fermi Golden rule rates, $\gamma_{L(R)}$, for ET from the level to the leads $\gamma_{L(R)} = (2/\hbar)\Gamma_{L(R)}$. The main parameters of this model are $\varepsilon_0(V)$ and $\Gamma_{L(R)}$ (see Figure 6).

The Landauer model, summarized in eqs 1−4, is used in two ways. Reference 29 observed that upon the extraction of the Cu atom from Az (Holo → Apo), the current is reduced by two orders of magnitude for a large range of temperatures (see Figure 1). Thus for Holo-Az, Cu seems to provide the most important transmission channel. For this reason, when modeling Holo-Az via eqs 1 and 2, the level energy $\varepsilon_0(V)$ will be interpreted as a Cu state energy. $H_{L(R)}$ will be interpreted as the through-Az tunneling matrix elements between the Cu level and the L(R) electrodes. In this case, eqs 1 and 2 describe an (off-) resonant tunneling model (through Cu).

For the case of Apo-Az, the Az/ligand supramolecule seems to be a deep tunneling barrier for a wide range of temperatures (thus the current reduction in Figure 1a,b). Because Apo-Az contains many amino acids with several levels providing tunneling transmission channels, $\varepsilon_0(V)$ cannot be interpreted as a single Az protein (amino acid) electronic level. Therefore, in eq 3, $\varepsilon_0(V)$ is taken to be an effective parameter that modulates the overall tunneling barrier provided by the molecule. When $\varepsilon_0(V) \gg \mu_{L(R)}$, the model describes an off-resonant tunneling mechanism through the Az amino acids. When $\varepsilon_0(V) \approx \mu_{L(R)}$, the model describes a resonant tunneling mechanism through the Az amino acids. We will also consider generalizations of the Landauer model that incorporate single and multiple fluctuating resonances. These more general models may be collectively described as descriptions of thermally modulated coherent tunneling.[44−46] They will be used to explore mostly the high-temperature regime of the Apo-Az experiments.[29]

Because for Holo-Az the Cu atom plays a central role for the transmission, we also need to consider the possibility that Cu provides a fully incoherent transmission channel. The length of the molecular bridge (30 Å) gives us the right to consider the ET as a hopping process, involving reversible transitions between the two oxidation states of the bridge (oxidized and reduced Cu electronic states) (see Figure 7) and the L(R) electrodes. Thus an alternative model used for Holo-Az is the one-site hopping model (incoherent model), where the hopping site is a Cu level. For the case of the hopping model, Cu acts as a redox site with reorganization energy λ (see Figure 7). This means that when the electron reaches the Cu atom, it remains there for sufficient time to reorganize the Cu-Az ligands. The steady-state current per molecule is given by

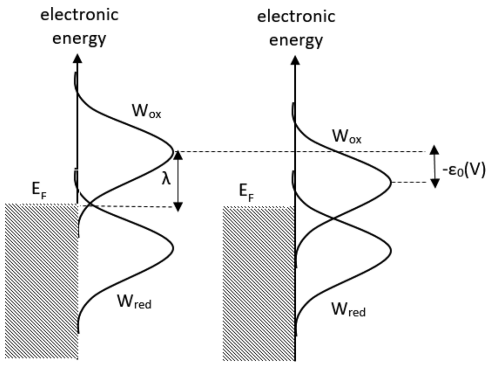

Figure 7. Reorganization energy, λ, distributions W_{ox} and W_{red} at equilibrium (left) and after application of a cathodic overpotential.

$$I(V) = -e\frac{k_L^{\rightarrow}(V)k_R^{\rightarrow}(V) - k_L^{\leftarrow}(V)k_R^{\leftarrow}(V)}{k_L^{\rightarrow}(V) + k_L^{\leftarrow}(V) + k_R^{\rightarrow}(V) + k_R^{\leftarrow}(V)} \quad (5)$$

DOI: 10.1021/acs.jpcc.9b00135
J. Phys. Chem. C 2019, 123, 5907−5922

where $k^{\rightarrow}_{L(R)}$ and $k^{\leftarrow}_{L(R)}$ are hopping rates to Cu from L(R) leads and from Cu to L(R) leads. When the Az−electrodes couplings are weak, so that the time scale for ET is long relative to that of thermal relaxation, each hopping step is associated with a rate obtained with the framework of the Marcus heterogeneous ET theory[13,14,20,35,36]

$$\vec{k}_L(V) = 2\frac{\Gamma_L}{\hbar}\int dE\, f(E-\mu_L)W_{ox}(\varepsilon_0(V),\mu_L)$$
$$\vec{k}_R(V) = 2\frac{\Gamma_R}{\hbar}\int dE\, f(E-\mu_R)W_{ox}(\varepsilon_0(V),\mu_R)$$
$$\vec{k}_L(V) = 2\frac{\Gamma_L}{\hbar}\int dE\, [1-f(E-\mu_L)]W_{red}(\varepsilon_0(V),\mu_L)$$
$$\vec{k}_R(V) = 2\frac{\Gamma_R}{\hbar}\int dE\, [1-f(E-\mu_R)]W_{red}(\varepsilon_0(V),\mu_R) \quad (6)$$

In the equations above, $W_{ox}(\varepsilon_0(V), \mu_{L(R)})$ and $W_{red}(\varepsilon_0(V), \mu_{L(R)})$ are distribution functions[35] for Cu oxidation and reduction, respectively (see Figure 7) and are given by

$$W_{ox}(\varepsilon_0(V),\mu_{L(R)}) = \frac{1}{\sqrt{4\pi\lambda k_B T}} e^{-(\lambda-(\mu_{L(R)}+E)+\varepsilon_0(V))^2/4\lambda k_B T}$$
$$W_{red}(\varepsilon_0(V),\mu_{L(R)}) = \frac{1}{\sqrt{4\pi\lambda k_B T}} e^{-(\lambda+(\mu_{L(R)}+E)-\varepsilon_0(V))^2/4\lambda k_B T} \quad (7)$$

The chemical potentials of the L(R) electrode are set to $\mu_L = -eV/2$ ($\mu_R = +eV/2$).

The main parameters used in this model are Cu's site energy, $\varepsilon_0(V)$, and the reorganization energy, λ, for the oxidation/reduction of Cu and $\Gamma_{L(R)}$ arising from the electrodes to Cu tunneling couplings through Az amino acids (see Figure 7).

We will also consider generalizations of the above incoherent hopping model to multisite hopping through the Az monolayer. This generalization will be necessary for describing the temperature dependence of Apo-Az in the T > 200 K region (see Figures 1a and 8). In addition to the above simplest models that represent the extremes of coherent and incoherent transport, we have also tested models describing intermediate regimes and containing relatively few parameters. These are the extended fully adiabatic Newns−Anderson model[37−40] and the two-step vibrationally coherent ET model (2sETm),[41,42] and they are described in the Supporting Information.

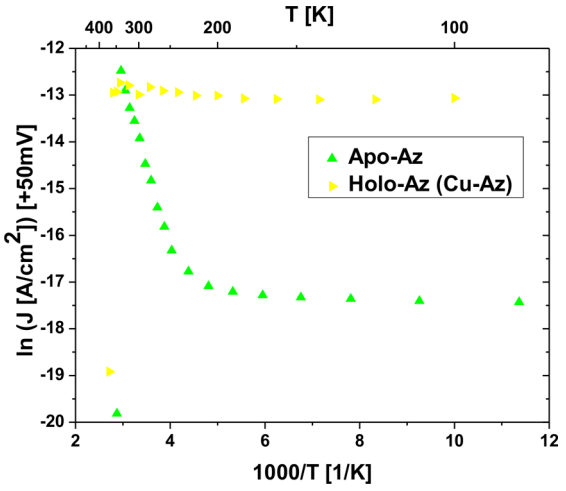

Figure 8. Experimental ln(J) versus 1000/T of Apo- and Holo-Az junction at +50 mV bias.[29]

3. RESULTS AND DISCUSSION

3.1. Modeling of Holo-Az Heterojunctions in Experiments I and II. *3.1.1. Experiment on Si-Oxide Substrate−Az−Au LOFO Heterojunctions (Exp. I).* Figure 1a,c shows the temperature dependence of ln(J) ($J = I_{total}/A$) for Apo-Az (Figure 1a) and Holo-Az (Figure 1c) for a wide range of bias voltages. In the case of Apo-Az, the current decreases with decreasing temperature for $T > T_c$ (T_c = 200 K) and then becomes temperature-independent. T_c remains the same for all voltages. Transport via Holo-Az is orders of magnitude greater than that via Apo-Az (apart from the highest temperatures, when the Holo- and Apo-Az currents are similar). Furthermore, the Holo-Az current is temperature-independent for all temperatures (T = 100−400 K) and all voltages ($|V|$ = 0.05 to 1.0 V).

Figure 8 is an example comparison of the Holo- and Apo-Az currents as a function of temperature for a specific voltage value (V = +50 mV). This figure shows the switch at T > 200 K from temperature independence to temperature dependence (activated transport) in the case of Apo-Az. The activation energy for thermally activated transport is $E_a \approx$ 250−255 meV.

The large enhancement of the current due to the addition of Cu (Apo → Holo) observed in ref 29 (Figure 8) indicates that Cu is the most important transmission channel for Holo-Az. Thus for Holo-Az, Cu is likely to act as a near-resonant/resonant tunneling or incoherent hopping site. In the following, we attempt to fit the temperature and voltage dependencies of the Holo-Az current using the simplest one-level coherent model (eqs 1−4) and the one-level incoherent hopping model (eqs 5−7). The best-fit parameters for both models are derived from the low-bias regime for which we do not expect the electric field to perturb the structures of the proteins in the monolayer.

Figures 9 and 10 show representative simultaneous fits of the temperature and voltage dependencies of the current measured in ref 29 using the coherent tunneling model (eqs 1−4) with a common set of parameter values. Figure 9 shows the ln(J)−T fitting for V = ±50 and 250 mV, and Figure 10a shows the ln(J)−V fitting at T = 300 K. The common parameter values derived from these fits are ε_0 = 0.03 eV, α = 0.75, $\Gamma_L = 3.3 \times 10^{-5}$ eV, and Γ_R/Γ_L = 10−1000 (the Fermi level at zero bias is 0 eV). We find that there is not much flexibility in the ε_0 value, which affects both the voltage and temperature dependence. There is more flexibility in the $\Gamma_{L(R)}$ values due to the uncertainty about the exact number of proteins in the system, $N_{contact}$. Thus the best-fit of the coherent tunneling model predicts a very low tunneling barrier at zero bias, as expected by the large enhancement seen in the current for Holo-Az as compared with Apo-Az.

Figure 9 shows that the current can be near-temperature-independent for the resonant tunneling regime. This is an expected feature of this regime,[19] only if $k_BT \leq \Gamma_L + \Gamma_R$, $\varepsilon_0(V)$, which turns out to be the case for the experimental temperature range and for the above-mentioned best-fit parameters. Figure 10a shows that the resonant tunneling channel that reproduces the low-bias experimental results cannot reproduce the high-bias current. This feature is

DOI: 10.1021/acs.jpcc.9b00135
J. Phys. Chem. C 2019, 123, 5907−5922

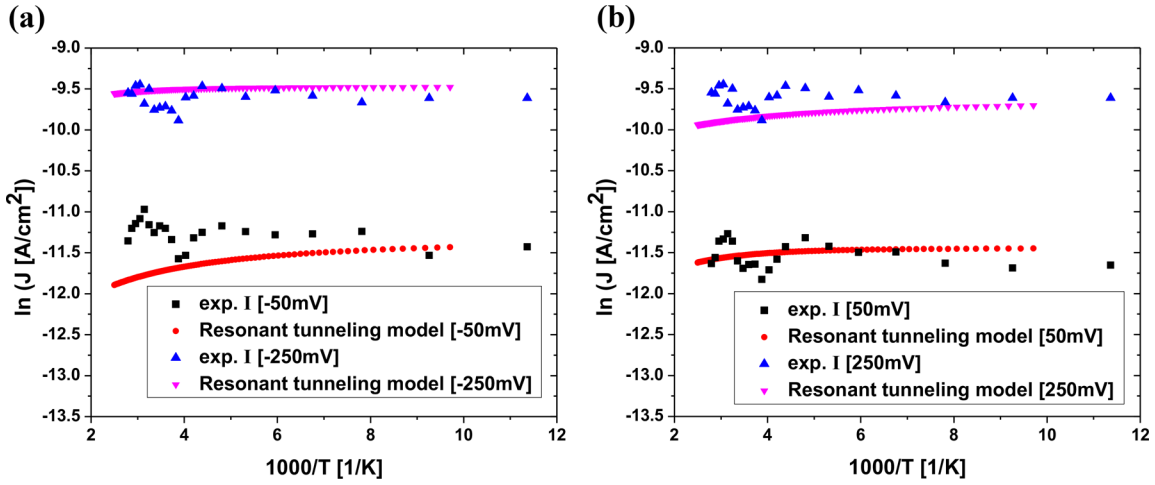

Figure 9. Experimental ln(J) versus 1000/T of Cu-Az (Holo-Az)[29] for different bias voltages versus theoretical predictions (eqs 1−4). (a) Bias voltages of −50 and −250 mV and (b) bias voltages of +50 and +250 mV. Parameter values of eqs 1−4 for all graphs: ε_0 = 0.03 eV, α = 0.75, Γ_L = 3.3 × 10^{-5}eV, and Γ_R/Γ_L = 1000.

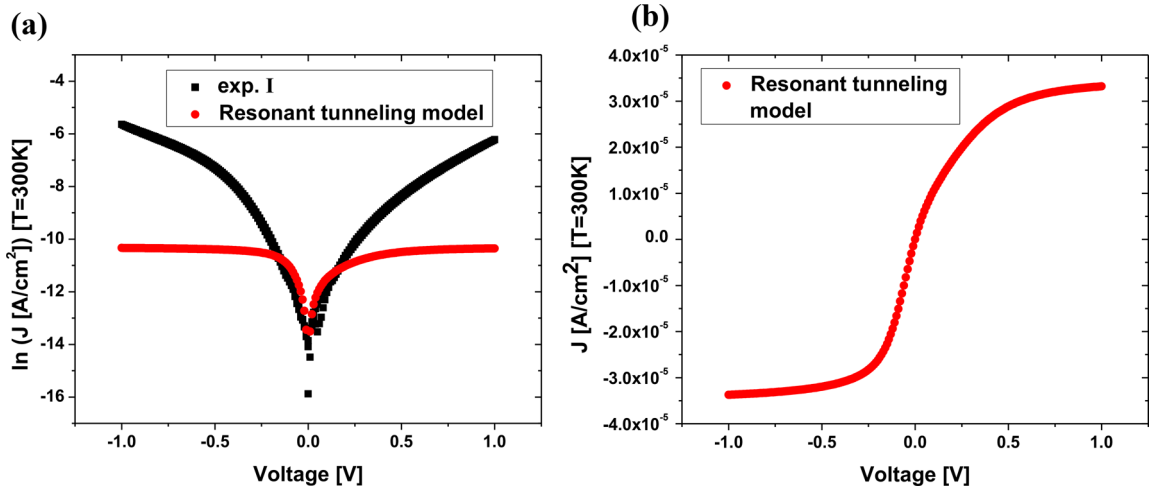

Figure 10. (a) Experimental ln(J) versus voltage of Cu-Az[29] at T = 300 K and theoretical best fit using the single-channel resonant-tunneling model (eqs 1−4) with the best-fit parameter values of ε_0 = 0.03 eV, α = 0.75, Γ_L = 3.3 × 10^{-5} eV, and Γ_R/Γ_L = 1000, as in Figure 9. The fit fails for bias voltages beyond 250 mV. This is because the current of a single resonant tunneling channel will saturate at higher bias voltages. (b) Theoretical resonant tunneling J versus voltage of Cu-Az at T = 300 K showing the saturation of the current at higher voltages for the best-fit parameters. Because the resonant tunneling current in this parameter regime is largely temperature-independent for T = 100−400 K, the shape of the J−V curve will not be altered within the experimental temperature range.

expected for a single-channel resonant tunneling current, which tends to saturate at high enough voltages.

Although it is tempting to adopt an off-resonant tunneling model (high ε_0 in eq 3), which is known to give temperature independence,[19] such a model completely fails to predict the low-bias voltage profile of the experiments in ref 29. A representative example is shown in Figure 11, which shows a typical ln(J)−V best fit for a one-level coherent tunneling model, where the level energy is high (ε_0 = 0.8 eV), such that the current is temperature-independent at all voltages. Figure 11 clearly demonstrates that such a model can reproduce the experimental results only at very low voltages.

Figures 12 and 13 are representative simultaneous fits of the temperature and voltage dependencies of the current measured in ref 29 using the incoherent one-site hopping model (eqs 5−7) with a common set of parameter values given by λ = 0.2 eV, α = 0.75, ε_0 = 0.01 to 0.03 eV, Γ_L = 1.0 × 10^{-5} to 1.0 × 10^{-3} eV, and Γ_R/Γ_L = 10−1000. Figure 12 shows ln(J)−T fits for V = ±50 and 250 mV, and Figure 13a shows the ln(J)−V fitting at T = 300 K. The range of values of our fit parameters is due to the uncertainty about the exact number of proteins in the system, $N_{contact}$. The one-site hopping model thus predicts a near-resonant Cu level at zero bias that enters the Fermi window at nonzero bias. It also predicts a low reorganization energy for the Cu redox site, which is consistent with inner sphere redox reorganization energies in azurin.[47] Both of these features are necessary to give a near-temperature-independent current at the various voltages[36] (Figure 12). The model simultaneously reproduces the ln(J)−V behavior for bias values up to ±250 mV (Figure 13a). Beyond the ±250 mV bias, the one-level hopping current saturates (Figure 13b), as expected.

A comparison of the ln(J)−V fits obtained using the coherent resonant tunneling (Figure 10a) to the fits obtained from the resonant single-channel hopping model (Figure 13a) shows that the one-site hopping model gives a better fit for a wider range of bias voltages; however, both models fail to

DOI: 10.1021/acs.jpcc.9b00135
J. Phys. Chem. C 2019, 123, 5907−5922

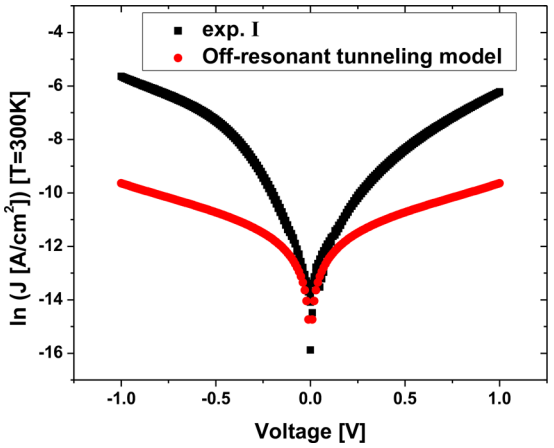

Figure 11. Experimental $\ln(J)$ versus voltage of Cu-Az[29] at T = 300 K and theoretical best-fit using the off-resonant tunneling model (eqs 1−4) with the best-fit parameter values of ε_0 = 0.8 eV, α = 0.5, Γ_L = 3.3 × 10^{-4} eV, and Γ_R/Γ_L = 1000.

reproduce the high-bias currents because both predict current saturation. We were also not able to reproduce the experimental results by global fitting using more complex models such as Newns−Anderson[37−40] or 2sETm.[41,42] (See the Supporting Information for a description of these models.)

The conclusion that a through-Cu resonant hopping model (with a low reorganization energy of 0.1 to 0.2 eV) can reproduce the low-bias Holo-Az currents of ref 29 is consistent with previous modeling of EC-STM experiments on Holo-Az molecular junctions.[28] Furthermore, the reorganization energy values predicted by our fitting using the through-Cu hopping model are consistent with ab initio and molecular dynamics computations of inner-sphere reorganization energies for the Cu ion in blue copper proteins.[17,47,48] (The systems we study are not in aqueous environment, so we expect the reorganization energy to be inner-sphere.) Recent experiments on small-molecule systems[49] clearly demonstrate transport via a hopping mechanism. A very recent experimental work on azurin-based molecular junctions[50] showed that by weakening the coupling between the protein and the gold electrodes the amount of inelastic current increases. This trend clearly suggests that in experiments like those of ref 29, which involve linkers that weaken the Cu−electrode couplings, the current may well proceed incoherently through the molecules.

The analysis in Figures 9−13 shows that the high-bias current observed in ref 29 cannot be due to a single resonant $\varepsilon_0(V)$ transport channel. Because the current does not saturate, additional resonant $\varepsilon_0(V)$ channels in the protein monolayer must come into resonance at higher voltages.[36] In the monolayer, different proteins are expected to have slightly different orientations, conformations, and local environments. Therefore, the Cu energy levels of the different Holo-Az proteins at zero bias will have a range of values (which are expected to be closer to the Fermi level as compared with the amino acids; see Table 1). Figure 14a illustrates this idea, where $\varepsilon_{0,k}$ refers to the zero-bias Cu-level energy of protein k in the monolayer. Given the fact that we were able to fit the voltage dependence of the current for the lower bias voltages with single-channel (single ε_0 value) models (Figures 9, 10, 12, and 13), a fraction of the energies $\{\varepsilon_{0,k}\}$ should be quasi-resonant with the Fermi level at zero bias. However, because $\varepsilon_{0,k}(V) = \varepsilon_{0,k} + (\alpha - 1/2)$ eV, for high-enough bias, more Cu levels in the monolayer ensemble will enter the Fermi window (Figure 14b), providing the monolayer with additional transport channels and avoiding a saturation of the monolayer current at high voltages (Figure 14b).

To test in the simplest manner this multichannel hypothesis for both the resonant tunneling and hopping mechanisms, we describe the monolayer (ensemble) current in terms of the following formula

$$J_{\text{multi}} = \underbrace{J(\varepsilon_{0,1}(V))}_{\text{low bias channel}} + \sum_{k\neq 1} P_k J(\varepsilon_{0,k}(V)),\ \ \varepsilon_{0,k\neq 1} > \varepsilon_{0,1} \tag{8}$$

On the right-hand side of this equation, the J values are current densities that are computed by either eqs 1−4 (coherent tunneling) or eqs 5−7 (incoherent hopping). The subscript "multi" means multi-$\varepsilon_0(V)$ sum. The first $J(\varepsilon_{0,1}(V))$ is computed using the zero-bias ε_0 value and the other parameter values that produce the low-bias fits in Figures 9 and 10 (for the coherent model) or Figures 12 and 13 (for the incoherent model). The remaining J values are computed by using a range

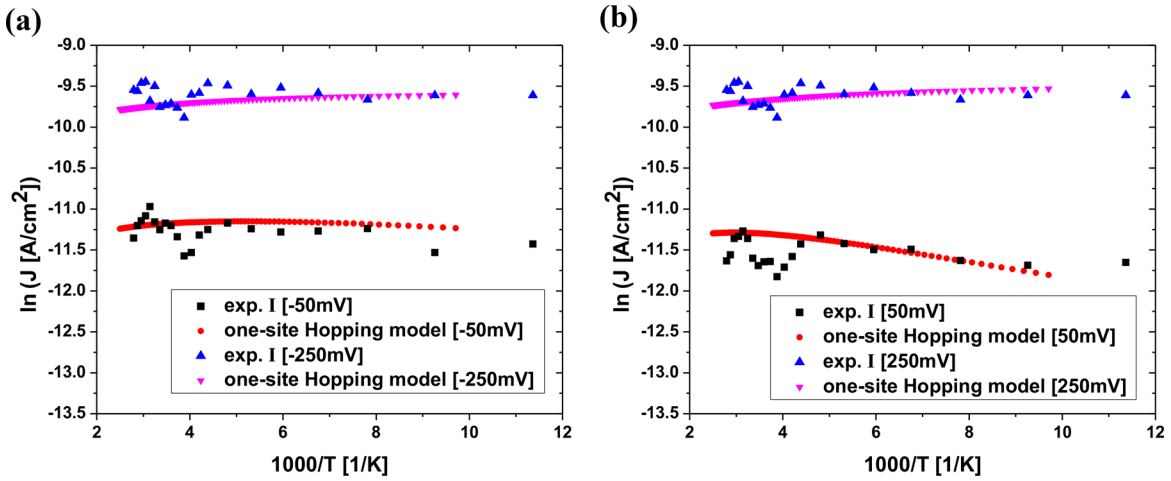

Figure 12. Experimental $\ln(J)$ versus $1000/T$ of Cu-Az (Holo-Az)[29] for different bias voltages versus theoretical best-fit using the one-site hopping model (eqs 5−7). (a) Bias voltages of −50 and −250 mV. (b) Bias voltages of +50 and +250 mV. The parameter values of eqs 5−7 for all graphs are λ = 0.2 eV, α = 0.75, ε_0 = 0.01 eV, Γ_L = 1.0 × 10^{-4} eV, and Γ_R/Γ_L = 1000.

DOI: 10.1021/acs.jpcc.9b00135
J. Phys. Chem. C 2019, 123, 5907−5922

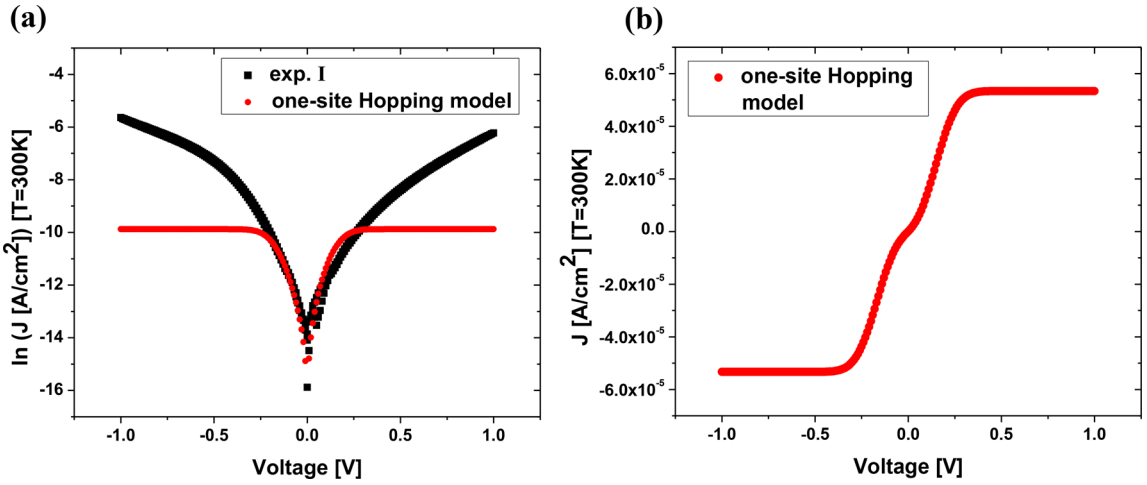

Figure 13. (a) Experimental $\ln(J)$ versus voltage of Cu-Az[29] at T = 300 K and theoretical best fit using the one-site hopping model eqs 5−7 (parameter values: λ = 0.2 eV, α = 0.75, ε_0 = 0.01 eV, $\Gamma_L = 1.0 \times 10^{-4}$ eV, and Γ_R/Γ_L = 1000). (b) Theoretical single-channel resonant hopping J versus voltage of Cu-Az at T = 300 K for the same parameter values, showing saturation behavior of the current. The behavior does not qualitatively change with temperature because the model predicts temperature-independent transport for T = 100−400 K (Figure 12).

Table 1. Conversion of Reduction Potentials versus SHE (mV) into Electronic Energies with Respect to Vacuum (eV) for Metals Relevant to Experiments I and II and for Some Amino Acids[50,54−58]

reactions	reduction potential ΔG_X^0 vs SHE (mV)	reduction potential ΔG_X^0 with respect to vacuum (eV)
Cu^{2+}/Cu^{+}(azurin)	310	−4.75
Cu^{2+}/Cu^{+}	160	−4.6
Ni^{2+}/Ni	−257	−4.18
Co^{2+}/Co	−277	−4.16
Zn^{2+}/Zn	−760	−3.68
	Amino Acids (at pH 7)	
Gly	1225	−3.215
Trp	1250	−3.19
Cys	1300	−3.14
Tyr	1350	−3.09

of higher zero-bias-level energies $\varepsilon_{0,k\neq1}$ = 0.1 to 0.5 eV, with all other parameters fixed to the values of the low-bias channel. The prefactors, P_k, are calculated from fitting to the experimental $\ln(J)-V$ for the whole range of experimental voltages using multiple regression analysis. P_k can be interpreted as the zero-bias ratio of population of proteins in the ensemble with a given $\varepsilon_{0,k\neq1}$ to the population of proteins with $\varepsilon_{0,1}$.

Figure 15 shows the individual J values in eq 8 for the coherent (Figure 15a) and the incoherent hopping (Figure 15b) models for a similar range of $\varepsilon_{0,k}$ values. The bias saturation behaviors of the current in the two mechanisms are very different. Figure 16 shows the monolayer (ensemble) current obtained from eq 8 for both mechanisms using the identical zero-bias-level energies, $\varepsilon_{0,k\neq1}$. Figure 16a is a representative fit of the $\ln(J)-V$ dependence measured in ref 29 using the incoherent multichannel hopping model, and Figure 16b shows the fit results using the coherent multichannel tunneling model. The hopping model of eq 8 gives a much better fit for a wider range of bias voltages, up to V = ±0.75 V, after which saturation starts. (To avoid saturation, more $\varepsilon_{0,k\neq1}$ should be added.)

On the contrary, the tunneling model of eq 8 begins to saturate at much lower voltages and also shows an asymmetry when reversing the voltage, not consistent with the experimental results. Both models give approximate temperature independence of the multichannel current (similar to Figures 9 and 12). We conclude that the dominant mechanism of Holo-Az transport in ref 29 for the whole range of bias voltages probed in the experiments is resonant through-Cu hopping.

3.1.2. Experiment on Au Microelectrode−Az−Au Microelectrode Heterojunctions (Exp. II). Reference 30 reported temperature-dependent current−voltage ($I-V$) measurements on Au(substrate)−Holo Az−Au (nanowire) junctions with a small number of proteins (nominally ~50). The currents were approximately temperature-independent (Fig-

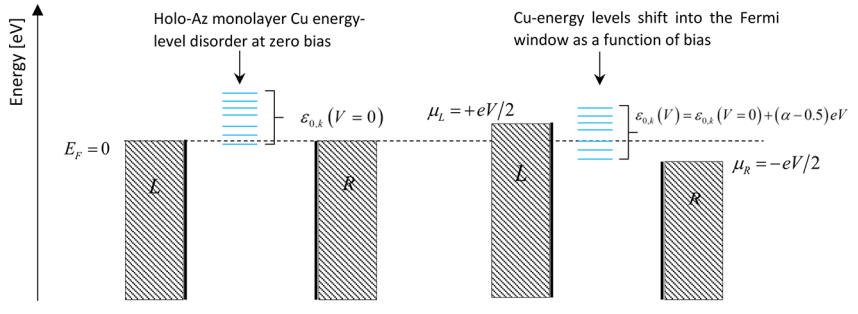

Figure 14. Schematic representation of the Cu-level multichannel hypothesis.

DOI: 10.1021/acs.jpcc.9b00135
J. Phys. Chem. C 2019, 123, 5907−5922

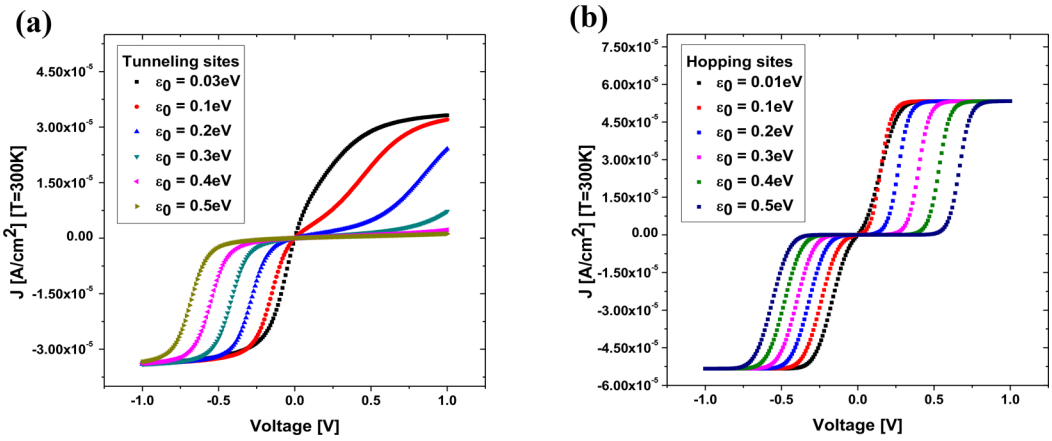

Figure 15. Theoretical J versus V of Cu-Az at T = 300 K using a range of energy levels, $\varepsilon_{0,k\neq1}$ = 0.1 to 0.5 eV (a) for the coherent resonant tunneling model (parameter values: $\varepsilon_{0,1}$ = 0.03 eV (best-fit at low-bias regime), α = 0.75, $\Gamma_L = 3.3 \times 10^{-5}$ eV, and Γ_R/Γ_L = 1000) and (b) for the incoherent hopping model (parameter values: $\varepsilon_{0,1}$ = 0.01 eV (best-fit at low-bias regime), λ = 0.2 eV, α = 0.75, $\Gamma_L = 1.0 \times 10^{-4}$ eV, and Γ_R/Γ_L = 1000).

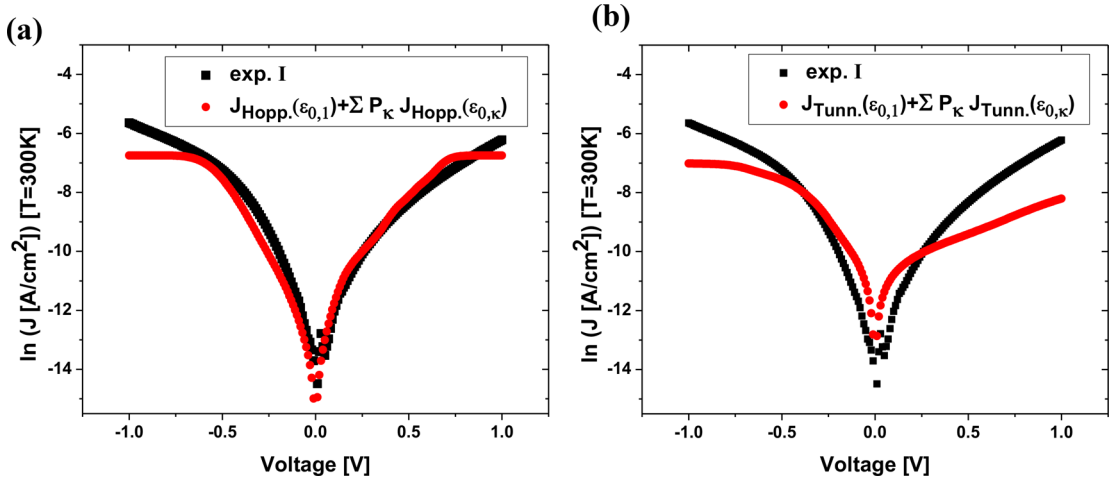

Figure 16. Experimental ln(J) versus voltage of Cu-Az[29] at T = 300 K and theoretical fits using the multichannel hypothesis of eq 8 using (a) the incoherent hopping mechanism (coefficients derived from multiple regression analysis: P_1 = 0.35, P_2 = 0.50, P_3 = 3.14, P_4 = 4.68, and P_5 = 13.01) and (b) the coherent tunneling mechanism (coefficients of multiple regression analysis: P_1 = 0.06, P_2 = 6.84, P_3 = 7.77, P_4 = 3.21, and P_5 = 7.68).

ures 3a,b). The $I-V$ curves are symmetric in contrast with the $J-V$ curves in ref 29.

We find that the $I-V$ experimental results of ref 30 can be reproduced by a single-channel coherent tunneling model (eqs 1−4), where the level energy is off-resonant to the Fermi level, ε_0, at zero bias. Typical ln(I)−T and ln(I)−V experimental and modeling plots are shown in Figures 17 and 18. The coherent tunneling model (eqs 1−4) parameter values that reproduce the experimental results are α = 0.470, ε_0 = 0.70 to 0.80 eV, $\Gamma_L = 1.1 \times 10^{-5}$ to 2.5×10^{-5} eV, and Γ_R/Γ_L = 100−1000.

In conclusion, the Holo-Az transport mechanisms differ in the two experiments,[29,30] as suggested by Figure 4. For the Holo-Az heterojunction in ref 29, the best low-bias fits to experiment are obtained by a one-channel resonant hopping model. To reproduce the high-bias currents, multiple resonant Cu-hopping channels must be introduced. For ref 30, a single-channel off-resonant tunneling model adequately describes the experimental results. These results are not that surprising given the structural differences between the heterojunctions in the two experiments. In the experiment of ref 30, the proteins in the monolayer are covalently bound to both leads. In the experiment of ref 29, the proteins in the monolayer are only

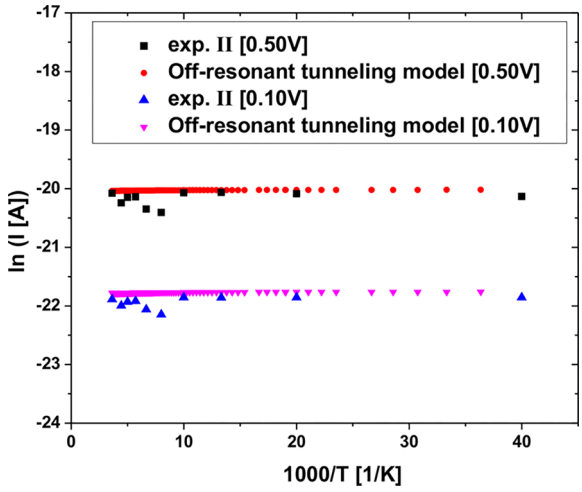

Figure 17. Experimental ln(I) versus 1000/T of Cu-Az[30] at +500 and +100 mV bias versus theoretical fits (eqs 1−4) using the parameter values: α = 0.470, ε_0 = 0.80 eV, $\Gamma_L = 1.15 \times 10^{-5}$ eV, and Γ_R/Γ_L = 1000.

DOI: 10.1021/acs.jpcc.9b00135
J. Phys. Chem. C 2019, 123, 5907−5922

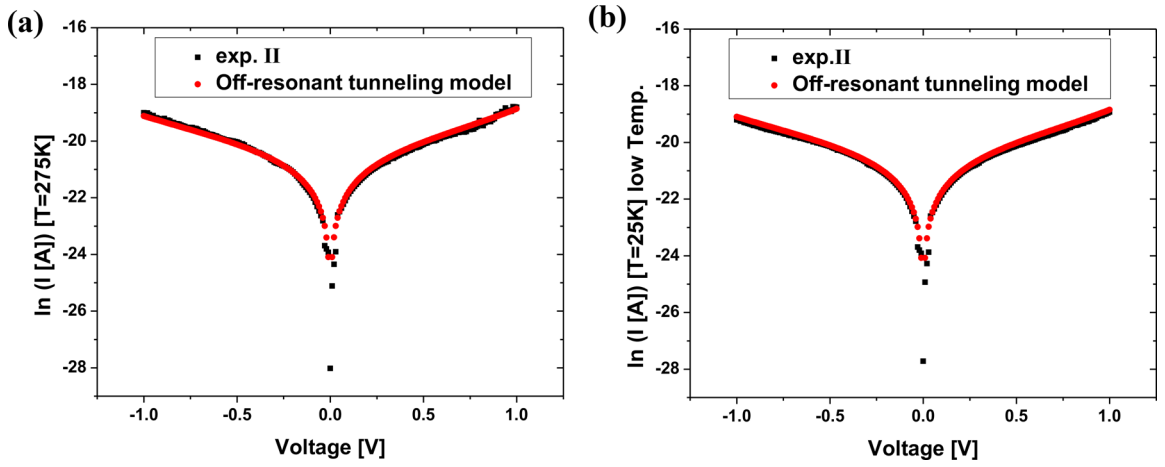

Figure 18. Experimental ln(I) versus voltage of Cu-Az[30] at (a) 275 and (b) 25 K versus theoretical fits (eqs 1−4) using the parameter values: α = 0.470, ε_0 = 0.80 eV, $\Gamma_L = 1.15 \times 10^{-5}$ eV, and Γ_R/Γ_L = 1000.

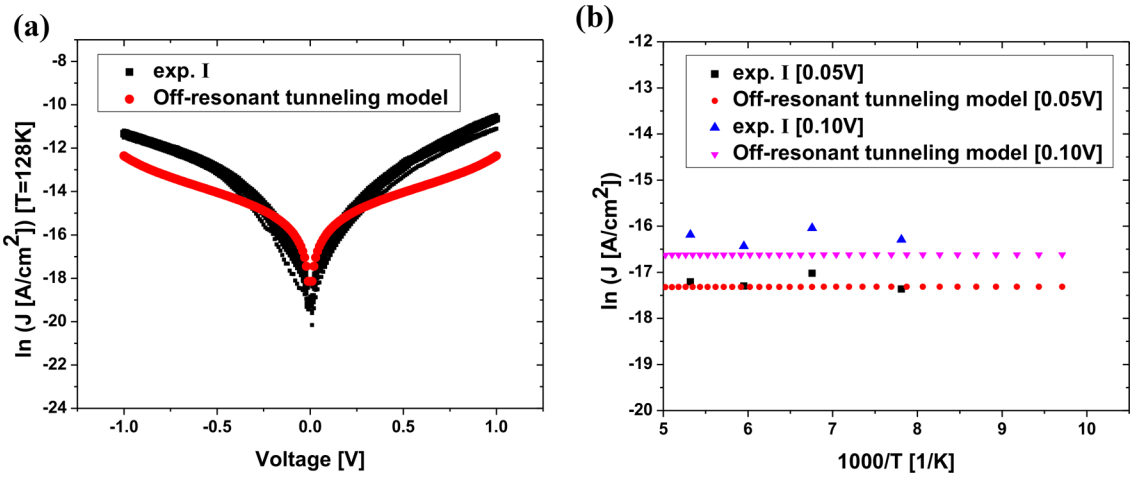

Figure 19. (a) Experimental ln(J) versus voltage of Apo-Az[29] at T = 128 K and theoretical fits using eqs 1−4. Because for 100 ≤ T ≤ 200 K the current is temperature-independent, the fit does not change with temperature. (b) Experimental ln(J) versus 1000/T of Apo-Az as a function of temperature at V = 0.05 and 0.10 V and theoretical fits using eqs 1−4. For both panels a and b, the parameter values in eqs 1−4 are α = 0.50, ε_0 = 0.70 eV, $\Gamma_L = 1.0 \times 10^{-3}$ eV, and Γ_R/Γ_L = 1.

covalently bound via a linker molecule to the substrate and are physisorbed to the Au LOFO. Thus, in the latter heterojunctions, there is much more disorder and weaker coupling of the metal to the leads (as compared with ref 30) both due to the physisorption and due to the linker molecule that increases the molecular bridge by ∼6 Å.

3.2. Modeling of Apo-Az Heterojunction Experiments (Exp. I). The modeling of Apo-Az experiments[29] is more involved. This is because two behaviors of the current as a function of temperature are observed. For T < 200 K, the temperature dependence of the current is largely flat, and for T > 200 K, the dependence is activated. It is notable that for the highest temperatures in the experiments (i.e., T = 400 K) the current for Apo-Az approaches the current for Holo-Az.

3.2.1. Low Temperatures ($T < T_c$). We find that the experimental results for the Apo-Az heterojunction in the temperature-independent regime (T < 200 K) can only be described via eqs 1−4 using an off-resonant tunneling model. Example comparisons of experiment and theory are shown in Figure 19. The parameter values employed for the fit are α = 0.50, ε_0 = 0.60 to 0.70 eV, $\Gamma_L = 1.0 \times 10^{-3}$ to 2.5×10^{-3} eV, and Γ_R/Γ_L = 1. The off-resonant tunneling behavior may be interpreted as a consequence of the fact that the proteins are missing the metal ion capable of localizing the charge (in a locally stable state).

In contrast with the case of Holo-Az, where ε_0 in eqs 2 and 3 was interpreted as a Cu-level energy, in the case of Apo-Az, ε_0 should be interpreted as an average amino-acid tunneling barrier.

3.2.2. High Temperatures ($T > T_c$). To reproduce the experimental results for the Apo-Az heterojunctions (ref 29, Figures 1a,b and 2) in the thermally activated transport regime (T > 200 K), we need a mechanism that shows activated current behavior and produces Apo-Az current for the highest temperatures that approach the Holo-Az currents (see Figure 8). This last observation implies that at the highest temperatures the protein (amino acids) provides channels (resonances) that are either within the Fermi window or can easily be accessed thermally. These resonances will be accessed by transferring charge either coherently or incoherently.

We find that the simple coherent transport model of eqs 1−4 cannot reproduce both the flat and the activated dependence of the Apo-Az current. The simplest generalization of this coherent model that incorporates a fluctuating

DOI: 10.1021/acs.jpcc.9b00135
J. Phys. Chem. C 2019, 123, 5907−5922

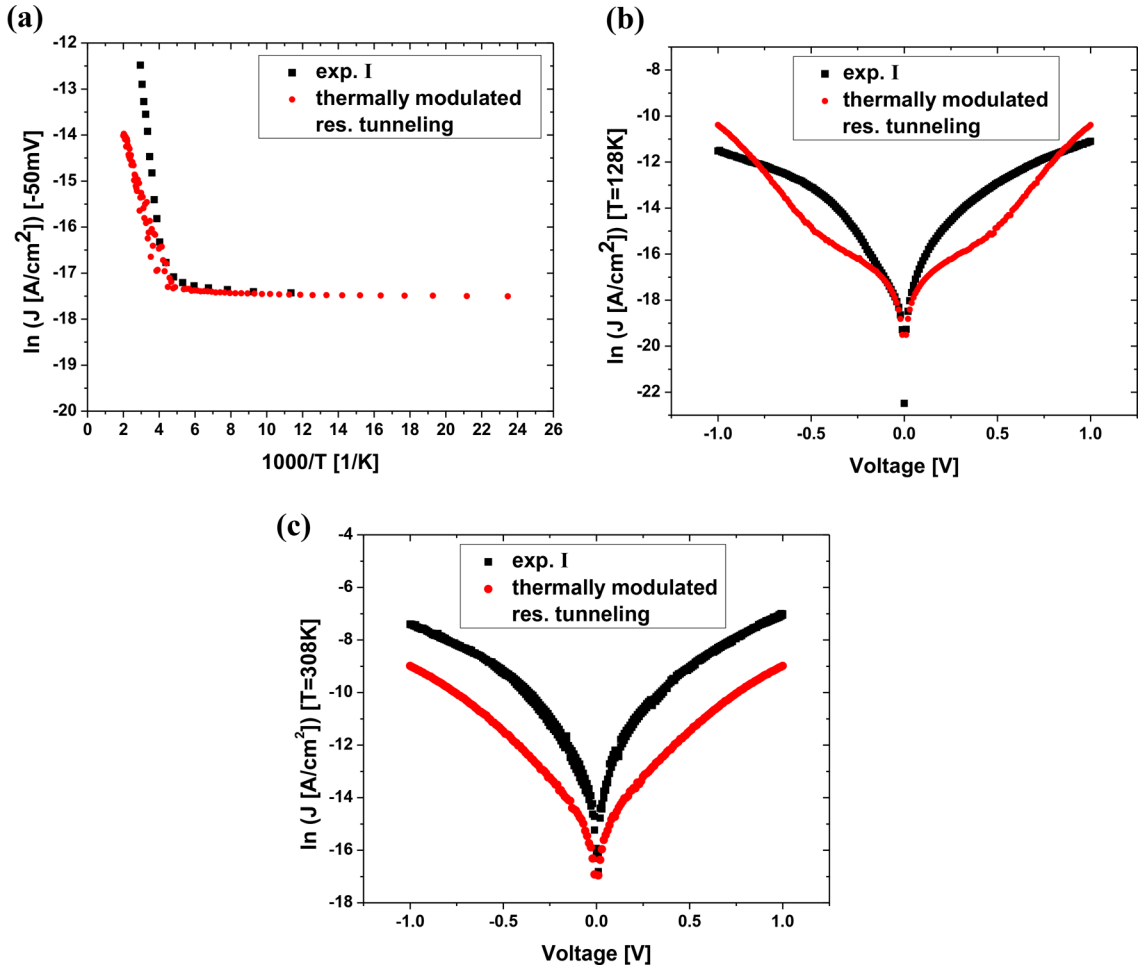

Figure 20. (a) Experimental ln(J) versus 1000/T of Apo-Az[29] as a function of temperature at $V = -0.05$ V versus theoretical fits (eqs 9 and 10). (b) Experimental ln(J) versus voltage of Apo-Az at $T = 128$ K (low-temperature regime) and theoretical fits using eqs 9 and 10. (c) Experimental ln(J) versus voltage of Apo-Az at $T = 308$ K (high-temperature regime) and theoretical fits using eqs 9 and 10. For all graphs, the parameter values are $\lambda = 1.1$ eV, $\alpha = 0.50$, $\varepsilon_0 = 0.60$ eV, $\Gamma_L = 1.0 \times 10^{-3}$ eV, and $\Gamma_R/\Gamma_L = 1$.

resonance is a thermally modulated tunneling model.[44−46] In this model, the level energy, ε_0, in eqs 2 and 3 is a stochastic variable with a Gaussian probability density

$$\rho(\varepsilon_0) = \frac{1}{\sqrt{2\pi}\sigma(T)} e^{-(\varepsilon_0-\bar{\varepsilon}_0)^2/2\sigma(T)^2} \quad (9)$$

where $\sigma(T) = \sqrt{\lambda_{eff} k_B T}$. ($\lambda_{eff}$ is an effective reorganization energy that characterizes the dependence of ε_0 level fluctuations as a function of temperature.) The measured mean current is an average over level fluctuations

$$\langle I(V)\rangle = \int_{-\infty}^{+\infty} d\varepsilon_0\, \rho(\varepsilon_0) I(V, \varepsilon_0) \quad (10)$$

where $I(V, \varepsilon_0)$ is the current per molecule based on the Landauer formalism (eqs 1−4). This model can partially reproduce the temperature dependence of the current in the thermally activated and the thermally independent regions for $\lambda_{eff} \approx 1.1$ eV and $\varepsilon_0 = 0.60$ eV and only for low-voltage values ($V \leq 0.250$ V) (see Figure 20a). However, the parameters that give the temperature dependence in Figure 20a cannot reproduce the experimental voltage dependence in the different temperature regimes (Figure 20b for $T = 128$ K and Figure 20c for $T = 308$ K).

As an alternative to the above model for the behavior of the Apo-Az currents at high T, we have also tested a multisite incoherent hopping model. To describe incoherent transport through the amino acids, we use a generalization of the one-site hopping model to N sites, where N is a parameter to be determined by fitting. This model[51,52] is schematically represented in Figure 21, where L(R) denotes the left

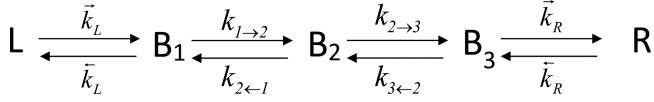

Figure 21. Schematic representation of the hopping model where a molecular bridge with $N = 3$ incoherent sites is coupled to the left (L) and right (R) electrodes.

(right) electron reservoirs (electrodes) and the B_i correspond to the different incoherent sites, each of which should be interpreted as an electronic level of energy, $\varepsilon_i(V)$, delocalized over one or more amino acids. The different $k_{i\to j}$ in this figure corresponds to the different (forward and backward) ET rates between these levels.

To determine the steady-state current in this model, we need to compute the stationary occupations ($\dot{P}_i^{(ss)} = 0$) in the

DOI: 10.1021/acs.jpcc.9b00135
J. Phys. Chem. C 2019, 123, 5907−5922

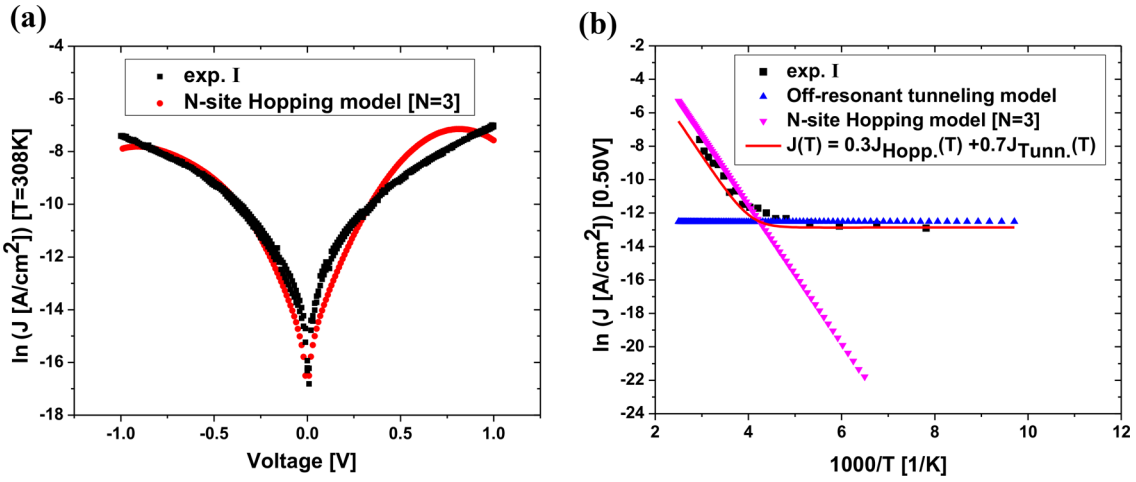

Figure 22. (a) Experimental ln(J) versus voltage of Apo-Az[29] at T = 308 K and theoretical fits (eqs 11−14). (b) Experimental ln(J) versus 1000/T of Apo-Az at V = 0.50 V over the entire temperature range and theoretical fits (using eqs 11−14 at high temperatures, eqs 1−4 at low temperatures, and eq 15 for both temperature regimes). Model parameter values of eqs 11−14: N = 3, λ = 0.3 eV, $\alpha_L = \alpha_R = -0.40$, ε_0 = 0.40 eV, $\Gamma = 3.30 \times 10^{-7}$ eV, $\Gamma_L = 3.30 \times 10^{-8}$ eV, and $\Gamma_R/\Gamma_L = 100$. Model parameter values of eqs 1−4: α = 0.50, ε_0 = 0.70 eV, $\Gamma_L = 1.0 \times 10^{-3}$ eV, and $\Gamma_R/\Gamma_L = 1$. Parameter value of eq 15 (red line): p = 0.3.

different sites (e.g., N = 3 below) by solving the corresponding kinetic equations

$$
\begin{aligned}
&-(\overleftarrow{k}_L + k_{1\to 2})P_1^{(ss)} + k_{2\leftarrow 1}P_2^{(ss)} + \vec{k}_L P_{L,R}^{(ss)} = 0\\
&k_{1\to 2}P_1^{(ss)} - (k_{2\leftarrow 1} + k_{2\to 3})P_2^{(ss)} + k_{3\leftarrow 2}P_3^{(ss)} = 0\\
&k_{2\to 3}P_2^{(ss)} - (k_{3\leftarrow 2} + \vec{k}_R)P_3^{(ss)} + \overleftarrow{k}_R P_{L,R}^{(ss)} = 0
\end{aligned}
\tag{11}
$$

The steady-state current per molecule (evaluated at the left interface) is simply given by

$$
I(V) = -e(\vec{k}_L P_{L,R}^{(ss)} - \overleftarrow{k}_L P_1^{(ss)}) \tag{12}
$$

To specify the voltage dependence of the molecular levels ($\varepsilon_i(V)$), we will assume that a portion $\alpha_{L,R}$ of the bias voltage drops at the left and the right metal−molecule interfaces, and a portion a_M drops along the molecule such that $a_L + a_M + a_R$ = 1.

For simplicity, we will assume that all of the forward rates are equal, $k_{i\to i+1} = k_f$. The same is true for the backward intramolecular rates, $k_{i\leftarrow i-1} = k_b$. The rates are given by

$$
k_{i\to j} = k e^{-(\varepsilon_i(V) - \varepsilon_j(V) + \lambda_i + \lambda_j)^2/4k_B T(\lambda_i + \lambda_j)} \tag{13}
$$

and they satisfy the detailed balance equation

$$
k_{i\to i+1}/k_{i\leftarrow i-1} = e^{-\Delta G_{i\to i+1}/k_B T} \tag{14}
$$

For the voltage-dependent rates involving charge transfer to the electrodes, we shall use the typical expressions taken from heterogeneous ET theory[13] in eqs 6 and 7. For hopping rates from/to the L(R) electrode, we use the molecular level coupled to the L(R) electrode, $\varepsilon_{1(N)}(V)$.

The main parameters used in this model are N (number of incoherent hopping sites), λ (reorganization energy), ε (the one-site energy of the molecular level at zero bias, assumed to be equal for all of them), k (zero-bias intramolecular transfer rate), $\alpha_{L,R}$ (parameters describing the voltage drop at the metal−molecule interfaces), and $\gamma_{L(R)} = (2/\hbar)\Gamma_{L(R)}$ (Golden rule rates).

We find that to reproduce the activated behavior of the Apo-Az current for T > 200 K, we need at least N = 3 incoherent sites in the molecular bridge (amino acid centers). An example comparison of experiment and N-site hopping theory is shown in Figure 22. Figure 22a compares the experimental ln(J)−V curve (black square) to a theoretical fit using the N = 3 hopping-site model (red circle). Figure 22b compares the experimental ln(J)−T curve to a theoretical fit using the same model (magenta triangle). The hopping model parameter values are λ = 0.3 eV (typical for amino acids[53]), $\alpha_L = \alpha_R$ = −0.40, ε_0 = 0.40 eV, $\Gamma_L = 1.0 \times 10^{-8}$ to 3.30×10^{-8} eV, Γ_R/Γ_L = 100, and $\Gamma = 1.0 \times 10^{-7}$ to 3.30×10^{-7} eV.

Because the N = 3 hopping-site model is not relevant to the low-temperature behavior, Figure 22b also shows a theoretical fit of the low-temperature regime using the off-resonant tunneling model (eqs 1−4) (blue triangle).

The fitting results suggest that the Apo-Az current at low temperatures is mediated by tunneling and that at high temperatures by through-amino-acid hopping. The simplest interpretation of the above is that the ensemble (monolayer) current density is described by the following simple relationship

$$
J_{total} = pJ_{Hopp.}(T) + (1 - p)J_{Tunn.}(T) \tag{15}
$$

where $J_{Hopp.}(T)$ is the current density through the N = 3 hopping sites at the high-temperature regime and $J_{Tunn.}(T)$ is the off-resonant tunneling current density. A good fit of eq 15 to the experimental temperature dependence for the whole range of temperatures is also shown in Figure 22b (red line).

If we consider that every protein in the ensemble may transport charge via two dominant channels, hopping and tunneling, then the prefactor p could be interpreted as the probability of hopping and $1 - p$ as the probability of tunneling. However, this probabilistic interpretation of the parameter may be an oversimplified picture given the approximate nature of the models. Equation 15 could also be interpreted as a result, emerging from a more complete, rigorous theory that reduces to the two limiting cases (tunneling, hopping) at different (low, high) temperatures.

3.3. Modeling Heterojunction Experiments of Zinc-, Cobalt-, and Nickel-Substituted Azurins (Exp. I). In addition to the Apo- and Holo-Az heterojunction experiments,

DOI: 10.1021/acs.jpcc.9b00135
J. Phys. Chem. C 2019, 123, 5907−5922

ref 29 reports the temperature and voltage dependencies of the current for Zn-, Ni-, and Co-substituted azurin heterojunctions. Figure 2 compares the current temperature dependencies of Apo-Az and Holo-Az to those of Zn-, Co-, and Ni-Az at a voltage of −50 mV. The current temperature dependencies all exhibit a temperature-independent region ($T < T_c$) and temperature-dependent (activated) region ($T > T_c$). The shapes of the $\ln(J)$ versus $1/T$ plots for Zn-, Co-, and Ni-Az are intermediates between those of Apo-Az and Holo-Az. The Zn-Az and Apo-Az heterojunctions have similar current temperature dependencies, and so do the Holo-Az and Ni-Az heterojunctions. The Co-Az current temperature dependence is approximately intermediate between the Apo-Az and Holo-Az extremes. As the medium is changed from Apo-Az to Zn-, Co-, Ni-, and Cu-substituted Az, the trend in the temperature dependence of the current is a reduction of the total current enhancement in the thermally activated region, that is, a reduction of $\Delta J^{act} = \ln(J_{max}) - \ln(J_{min}) \approx \ln(J(T_{max})) - \ln(J(T_{min}))$, with a simultaneous increase in the minimum current, $\ln(J_{min}) \approx \ln(J(T_{min}))$, in the temperature-independent region. This trend seems to be correlated with the reduction potentials versus SHE of the substituted metals and of some common amino acids (Table 1). The last column in Table 1 converts the reduction potentials versus SHE to an absolute energy scale (in electronvolts) with respect to vacuum,[50,54−58] to be compared with the Au Fermi level[59] of −5.1 eV. It is obvious from the table that the barrier ΔG^0_X for the reduction of a metal or of an amino acid (AA) X from Au follows the same trend as ΔJ^{act}_X, that is, $\Delta G^0_{Cu} < \Delta G^0_{Ni} < \Delta G^0_{Co} < \Delta G^0_{Zn} < \Delta G^0_{AA}$ and $\Delta J^{act}_{Cu-Az} < \Delta J^{act}_{Ni-Az} < \Delta J^{act}_{Co-Az} < \Delta J^{act}_{Zn-Az} < \Delta J^{act}_{Apo-Az}$.

Therefore, we expect that in going from Zn to Ni the ensemble-averaged barrier for tunneling through Az is progressively lowered if the metal participates in transport. Figure 23 shows fits of the experimental results for the cases of Ni-, Co-, and Zn-Az heterojunctions in the temperature-independent regime ($T < 200$ K) using the tunneling model (eqs 1−4) with different values of ε_0 that follow the trend of ΔG^0_X in Table 1. An example comparison of experiment and theory is shown in Figure 23. The parameter values employed for the fit are $\Gamma_L = 1.0 \times 10^{-3}$ to 2.5×10^{-3} eV, $\Gamma_R/\Gamma_L = 1$, $\alpha = 0.50$, and $\varepsilon_0 = 0.2$, 0.22, and 0.55 eV for Ni-, Co-, and Zn-Az heterojunctions, respectively (eqs 1−4).

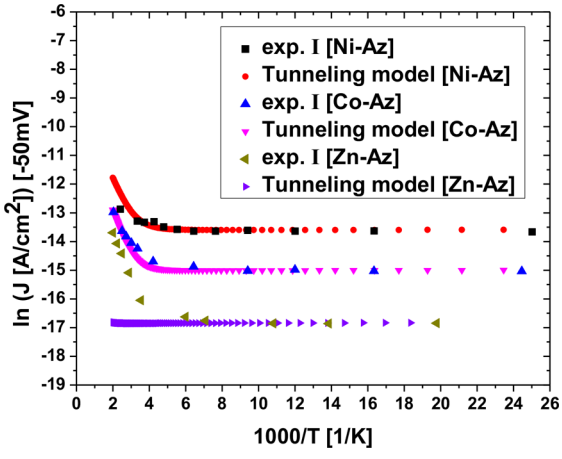

Figure 23. Experimental $\ln(J)$ versus $1000/T$ of Ni-, Co-, and Zn-Az[29] at −50 mV bias and theoretical best-fit using the off-resonant tunneling model (eqs 1−4) with the best-fit parameter values of $\Gamma_L = 1.0 \times 10^{-3}$ eV, $\Gamma_R/\Gamma_L = 1$, $\alpha = 0.50$, and $\varepsilon_0 = 0.20$, 0.22, and 0.55 eV for Ni-, Co-, and Zn-Az heterojunctions, respectively.

In the cases of Ni-Az and Co-Az heterojunctions, we can reproduce the experimental results both in the temperature-independent ($T < 200$ K) and thermally activated regimes ($T > 200$ K) using the Landauer model (eqs 1−4) with $\varepsilon_0 = 0.2$ eV (Ni) and $\varepsilon_0 = 0.22$ eV (Co). In the case of the Zn-Az heterojunction the current−temperature dependence resembles very much that of Apo-Az. This is reasonable because the reduction potential of Zn ($E^0 = -760$ mV vs SHE)[54] is relatively close to that amino acid redox potentials (e.g., Tyr, Cys, Trp, Gly) (see Table 1). Therefore, Zn does not provide a much better transport channel than the amino acids in azurin, and to explain the temperature behavior, we can adopt the same modeling as in Apo-Az. Figure 23 shows that the Zn-Az current in the temperature-independent region ($T < 200$ K) is reproduced by a tunneling model with $\varepsilon_0 = 0.55$ eV, but this model cannot reproduce the current in the thermally activated region ($T > 200$ K). For this region, we use the N-site hopping model, and as in the Apo-Az case we can reproduce the current for $N \geq 3$ (Figure 24).

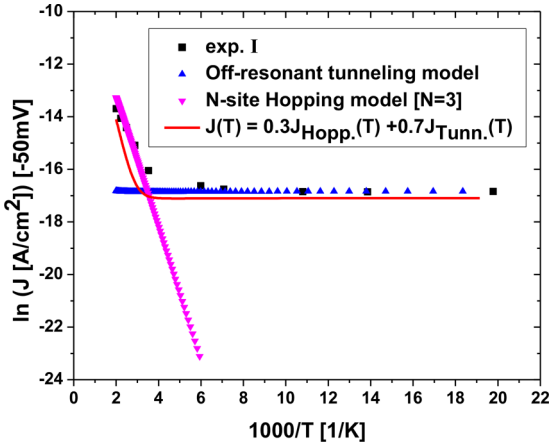

Figure 24. Experimental $\ln(J)$ versus $1000/T$ of Zn-Az[29] at $V = -50$ mV over the entire temperature range and theoretical fits (using eqs 11−14 at high temperatures, eqs 1−4 at low temperatures, and eq 15 for both temperature regimes). Model parameter values of eqs 11−14: $N = 3$, $\lambda = 0.3$ eV, $\alpha_L = \alpha_R = -0.40$, $\varepsilon_0 = 0.20$ eV, $\Gamma = 1.0 \times 10^{-12}$ eV, $\Gamma_L = 3.30 \times 10^{-8}$ eV, and $\Gamma_R/\Gamma_L = 1$. Model parameter values of eqs 1−4: $\alpha = 0.50$, $\varepsilon_0 = 0.55$ eV, $\Gamma_L = 1.0 \times 10^{-3}$ eV, and $\Gamma_R/\Gamma_L = 1$. Parameter value of eq 15 (red line): $p = 0.3$.

As in the case of Apo-Az, the hopping and tunneling currents can be combined to reproduce the Zn-Az current in the whole temperature range via eq 15. Figure 24 (red line) shows the monolayer Zn-Az current computed from eq 15 and compared with the experimental results of ref 29.

It should be noted that the temperature dependencies of the activated currents in Figure 2 for Ni-Az and Co-Az can also be reproduced by a through-amino-acid hopping model, as is the case of Apo- and Zn-Az. Given the fact that at the highest temperatures all currents in Figure 2 converge to similar values, the best interpretation of the activated region is that the current is dominated by through amino-acid hopping in all cases.

DOI: 10.1021/acs.jpcc.9b00135
J. Phys. Chem. C 2019, 123, 5907−5922

Table 2. Transport Mechanisms for the Azurin Heterojunctions[29,30] in the Different Temperature Regimes[a]

Holo-Az experiments[29,30]	Zn- and Apo-Az experiments[29]	Ni- and Co-Az experiments[29]
temp.-independent current	temp.-dependent current: $T > T_c$ temp.-independent current: $T < T_c$	current temp. dependence is intermediate between the Holo- and Apo-Az behaviors
Exp. I[29] through-Cu incoherent resonant hopping (high disorder)	$T < T_c$: off-resonant tunneling	$T < T_c$: near-resonant tunneling
Exp. II[30] off-resonant tunneling	$T > T_c$: through-amino-acid hopping	$T > T_c$: both near-resonant tunneling and through-amino-acid hopping are consistent with experiment

[a] $T_c \approx 200$ K remains the same for all azurin heterojunctions.

4. CONCLUSIONS

The present theoretical investigation is motivated by experiments[29,30] that measure the current−voltage and current−temperature dependencies of ETpr azurin monolayer heterojunctions. The experiments in ref 29 (exp. I) involve Si-oxide substrate−Az−Au or Hg LOFO heterojunctions and compare the voltage and temperature dependencies of Holo-Az (with Cu as the redox site) and Apo-Az (with Cu removed). They also measure the temperature dependencies of other metal-substituted azurins (Ni, Co, and Zn). The experiments in ref 30 (exp. II) involve Au microelectrode−Az−Au microelectrode heterojunctions and measure the current−voltage and current−temperature dependencies of Holo-Az. The experimental results are very interesting because they enable the analysis of transport through the same protein monolayer medium as a function of the metal substitution, temperature, and voltage.

In both types of heterojunctions,[29,30] the Holo-Az current is approximately temperature-independent, but the bias voltage dependence of the Holo-Az current in ref 29 differs considerably from that in ref 30. Furthermore, in contrast with the temperature-independent Holo-Az, the Apo-Az current in ref 29 shows activationless behavior at lower temperatures ($T < 200$ K) and activated behavior at higher temperatures ($T > 200$ K). The temperature dependencies of the current for the other metal-substituted azurin monolayers interpolate between the Holo-Az behavior and the Apo-Az behavior. In the temperature-independent regime, the magnitude of the current is the highest for Holo-Az and the lowest for Apo-Az, with the other metal-substituted azurins showing intermediate current values between the two extremes (Cu-Az > Ni-Az > Co-Az > Zn-Az > Apo-Az). At the highest temperatures, the current magnitudes of all azurin types are similar.

The richnesss of the above phenomenology offers an opportunity to explore transport mechanisms through the azurin monolayers and to gain insight into the competition between metal- and amino-acid-mediated transport in these systems. In our work, we have attempted to fit the experimental results using several standard models of coherent and incoherent transport mechanisms. Importantly, for each mechanism, we simultaneously fit both the voltage and temperature dependencies of the logarithm of the current using a common set of parameters. This approach turns out to limit to a large extent both the type of transport mechanism and its corresponding parameter set compatible with experiment. Our results do not exclude the possibility that the systems studied may operate in more complex, intermediate regimes between the extremes of fully coherent and fully incoherent transport. However, given the information we have about the systems, it is impossible to determine more precisely those regimes. Our results are summarized in Table 2.

We find that in the Holo-Az heterojunctions of ref 29 transport is mediated by through-Cu incoherent resonant hopping with the possibility of through-Cu coherent resonant tunneling also contributing for low-bias voltages. In contrast, for the Holo-Az heterojunctions in ref 30, transport is mediated by off-resonant tunneling. Our analysis also shows that the Cu-level energies of the Holo-Az monolayers in ref 29 are much more disordered compared with the monolayers in ref 30. These results explain the large differences in the low-bias voltage dependencies of the current per azurin molecule observed in the two experiments (Figure 4) and also are consistent with the structural differences between the two types of heterojunctions. The proteins in ref 29 are covalently bound via a linker molecule to one lead and physisorbed to the other. The proteins in ref 30 are covalently bound by S−Au bonds to both leads. Thus each Cu metal in the heterojunctions of ref 29 is on average much more weakly coupled to the leads as compared with ref 30, and the protein monolayer is much more disordered.

For the Apo-Az experiments,[29] we find that the removal of the Cu atom changes the transport mechanism to through-amino-acid off-resonant tunneling in the lower temperature (temperature-independent) regime and to through-amino-acid hopping in the higher temperature, activated regime. For the other metal-substituted azurins (Zn, Ni, Co), the off-resonant tunneling model reproduces the currents in the temperature-independent regime with average tunneling barriers that follow the same magnitude trend as the redox potentials of the metals, indicating that the metal type plays a role in influencing the average tunneling barrier in these systems. For the high-temperature, activated regime, through-amino-acid hopping can reproduce the current behavior for all three metal substitutions, although the off-resonant tunneling model can also reproduce the activated region for Ni- and Co-substituted azurins. The best self-consistent interpretation of the currents' temperature dependence at the highest temperatures in Apo-, Zn- Co-, and Ni-Az monolayers is a through-amino-acid hopping mechanism.

The variability and mixing of transport mechanisms in the protein heterojunctions (see Table 2) is consistent with our current understanding of biomolecular ET. Even at the single-molecule level, protein structural fluctuations can lead to fluctuating molecular and metal electronic-level energies and intralevel couplings, giving rise to a spread of ET rates/currents and to ET mechanism switches.[8,16,18,24,46,60] At the monolayer level, the situation is even more complex because there is additional static disorder. Furthermore, the dominance of the through-Cu hopping mechanism for the Holo-Az heterojunctions with weak metal−lead couplings is not surprising given the recent theoretical and experimental results on redox molecular junctions.[49,61,62] Our results show that when the redox hopping site is near-resonant to or within the Fermi

DOI: 10.1021/acs.jpcc.9b00135
J. Phys. Chem. C 2019, 123, 5907−5922

window and the reorganization is small (as is the case of the Cu level in the heterojunctions of ref 29), the hopping current can be near-temperature-independent for finite bias voltages. Therefore, a temperature-independent current does not necessarily imply a coherent tunneling mechanism, nor does it exclude a hopping mechanism. This conclusion is consistent with other theoretical works on hopping transport,[36] and it implies that additional experimental probes of the current (apart from the temperature and voltage dependencies) are necessary to determine transport mechanism.

■ ASSOCIATED CONTENT

Supporting Information

The Supporting Information is available free of charge on the ACS Publications website at DOI: 10.1021/acs.jpcc.9b00135.

Two more-complex models (PDF)

■ AUTHOR INFORMATION

Corresponding Author

*E-mail: skourtis@ucy.ac.cy.

ORCID

Juan-Carlos Cuevas: 0000-0001-7421-0682

Spiros S. Skourtis: 0000-0002-5834-248X

Notes

The authors declare no competing financial interest.

■ ACKNOWLEDGMENTS

S.V. and S.S.S. thank the University of Cyprus for Ph.D. Scholarship support. J.-C.C. thanks the Spanish MINECO (contract no. FIS2017-84057-P) for financial support. We thank N. Amdursky, J. Blumberger, D. Cahen, D. Marchak, I. Pecht, L. Sepunaru, M. Sheves, and A. Vilan for many helpful discussions.

■ REFERENCES

(1) Marcus, R. A.; Sutin, N. Electron Transfers in Chemistry and Biology. *Biochim. Biophys. Acta, Rev. Bioenerg.* **1985**, *811*, 265−322.

(2) Bendall, D. S. *Protein Electron Transfer*; Bios Scientific Publishers: Oxford, U.K., 1996.

(3) Canters, G. W.; Vijgenboom, E. *Biological Electron Transfer Chains: Genetics, Composition and Mode of Operation*; Springer: Dordrecht, The Netherlands, 1998.

(4) Jortner, J.; Bixon, M.; Prigogine, I.; Rice, S. A. *Electron Transfer - From Isolated Molecules to Biomolecules*; John Wiley & Sons: New York, 1999.

(5) *Long-Range Charge Transfer in DNA I and II*; Schuster, G. B., Ed.; Topics in Current Chemistry *236*−*237*; Springer: Berlin, 2004.

(6) Beratan, D. N.; Skourtis, S. S. Electron Transfer through Proteins. *Encyclopedia of Biophysics.* **2013**, 625−630.

(7) Winkler, J. R.; Gray, H. B. Electron Flow through Metalloproteins. *Chem. Rev.* **2014**, *114*, 3369−3380.

(8) Skourtis, S. S. Probing Protein Electron Transfer Mechanisms From the Molecular to the Cellular Length Scales. *Biopolymers* **2013**, *100*, 82−92.

(9) *Energy/Mechanistic Biology*; Beratan, D. N., Skourtis, S. S., Erb, T. J., Gerlt, J. A., Eds.; Current Opinion in Chemical Biology *47*; Elsevier, 2018; pp 1−142.

(10) Teo, R. D.; Rousseau, B. J. G.; Smithwick, E. R.; Di Felice, R.; Beratan, D. N.; Migliore, A. Charge Transfer between [4Fe4S] Proteins and DNA Is Unidirectional: Implications for Biomolecular Signaling. *Chem.* **2019**, *5*, 122−137.

(11) Balzani, V.; Piotrowiak, P.; Rodgers, M. A. J.; Mattay, J.; Astruc, D.; Gray, H. B.; Wrinkler, J.; Fukuzumi, S.; Mallouk, T. E.; Haas, Y.; et al. *Electron Transfer in Chemistry*; Wiley-VCH: Weinheim, Germany, 2001; Vols. *1*−*4*.

(12) Kuznetsov, A. M.; Ulstrup, J. *Electron Transfer in Chemistry and Biology: An Introduction to Theory*; John Wiley & Sons, Ltd.: Chichester, U.K., 1999.

(13) May, V.; Kuhn, O. *Charge and Energy Transfer Dynamics in Molecular Systems*, 3rd ed.; Wiley-VCH: Berlin, 2011.

(14) Nitzan, A. *Chemical Dynamics in Condensed Phases*; Oxford University Press, 2006.

(15) Beratan, D. N.; Skourtis, S. S.; Balabin, I. A.; Balaeff, A.; Keinan, S.; Venkatramani, R.; Xiao, D. Steering Electrons on Moving Pathways. *Acc. Chem. Res.* **2009**, *42*, 1669−1678.

(16) Skourtis, S. S.; Waldeck, D. H.; Beratan, D. N. Fluctuations in Biological and Bioinspired Electron-Transfer Reactions. *Annu. Rev. Phys. Chem.* **2010**, *61*, 461−485.

(17) Blumberger, J. Recent Advances in the Theory and Molecular Simulation of Biological Electron Transfer Reactions. *Chem. Rev.* **2015**, *115*, 11191−11238.

(18) Beratan, D. N.; Liu, C.; Migliore, A.; Polizzi, N. F.; Skourtis, S. S.; Zhang, P.; Zhang, Y. Charge Transfer in Dynamical Biosystems, or The Treachery of (Static) Images. *Acc. Chem. Res.* **2015**, *48*, 474−481.

(19) Cuevas, J. C.; Scheer, E. *Molecular Electronics: An Introduction to Theory and Experiment*, 2nd ed.; World Scientific: Singapore, 2017.

(20) Zhang, J.; Kuznetsov, A.; Medvedev, I. G.; Chi, Q.; Albrecht, T.; Jensen, P.; Ulstrup, J. Single-Molecule Electron Transfer in Electrochemical Environments. *Chem. Rev.* **2008**, *108*, 2737−2791.

(21) Amdursky, N.; Marchak, D.; Sepunaru, L.; Pecht, I.; Sheves, M.; Cahen, D. Electronic Transport via Proteins. *Adv. Mater.* **2014**, *26*, 7142−7161.

(22) Ruiz, M. P.; Aragonès, A. C.; Camarero, N.; Vilhena, J. G.; Ortega, M.; Zotti, L. A.; Pérez, R.; Cuevas, J. C.; Gorostiza, P.; Díez-Pérez, I. Bioengineering a Single-Protein Junction. *J. Am. Chem. Soc.* **2017**, *139*, 15337−15346.

(23) Skourtis, S. S.; Balabin, I. A.; Kawatsu, T.; Beratan, D. N. Protein Dynamics and Electron Transfer: Electronic Decoherence and Non-Condon Effects. *Proc. Natl. Acad. Sci. U. S. A.* **2005**, *102*, 3552−3557.

(24) Balabin, I. A.; Beratan, D. N.; Skourtis, S. S. Persistence of Structure Over Fluctuations in Biological Electron-Transfer Reactions. *Phys. Rev. Lett.* **2008**, *101*, 158102.

(25) Chi, Q.; Zhang, J.; Andersen, J.; Ulstrup, J. Ordered Assembly and Controlled Electron Transfer of the Blue Copper Protein Azurin at Gold (111) Single-Crystal Substrates. *J. Phys. Chem. B* **2001**, *105*, 4669−4679.

(26) Chi, Q.; Farver, O.; Ulstrup, J. Long-Range Protein Electron Transfer Observed at the Single-Molecule Level: In Situ Mapping of Redox-Gated Tunneling Resonance. *Proc. Natl. Acad. Sci. U. S. A.* **2005**, *102*, 16203−16208.

(27) Alessandrini, A.; Salerno, M.; Frabboni, S.; Facci, P. Single-Metalloprotein Wet Biotransistor. *Appl. Phys. Lett.* **2005**, *86*, 133902.

(28) Alessandrini, A.; Corni, S.; Facci, P. Unravelling Single Metalloprotein Electron Transfer by Scanning Probe Techniques. *Phys. Chem. Chem. Phys.* **2006**, *8*, 4383−4397.

(29) Amdursky, N.; Sepunaru, L.; Raichlin, S.; Pecht, I.; Sheves, M.; Cahen, D. Electron Transfer Proteins as Electronic Conductors: Significance of the Metal and Its Binding Site in the Blue Cu Protein, Azurin. *Adv. Sci. (Weinh).* **2015**, *2*, 1400026.

(30) Yu, X.; Lovrincic, R.; Sepunaru, L.; Li, W.; Vilan, A.; Pecht, I.; Sheves, M.; Cahen, D. Insights into Solid-State Electron Transport through Proteins from Inelastic Tunneling Spectroscopy: The Case of Azurin. *ACS Nano* **2015**, *9*, 9955−9963.

(31) Vilan, A.; Cahen, D. Soft Contact Deposition onto Molecularly Modified GaAs. Thin Metal Film Flotation: Principles and Electrical Effects. *Adv. Funct. Mater.* **2002**, *12*, 795−807.

(32) Smith, P.; Nordquist, C.; Jackson, T.; Mayer, T.; Martin, B.; Mbindyo, J.; Mallouk, T. Electric-Field Assisted Assembly and Alignment of Metallic Nanowires. *Appl. Phys. Lett.* **2000**, *77*, 1399−1401.

DOI: 10.1021/acs.jpcc.9b00135
J. Phys. Chem. C 2019, 123, 5907−5922

(33) Freer, E.; Grachev, O.; Duan, X.; Martin, S.; Stumbo, D. High-Yield Self-Limiting Single-Nanowire Assembly with Dielectrophoresis. *Nat. Nanotechnol.* **2010**, *5*, 525−530.
(34) Garg, K.; Ghosh, M.; Eliash, T.; van Wonderen, J.; Butt, J.; Shi, L.; Jiang, X.; Zdenek, F.; Blumberger, J.; Pecht, I.; et al. Direct Evidence for Heme-Assisted Solid-State Electronic Conduction in Multi-Heme c-Type Cytochromes. *Chem. Sci.* **2018**, *9*, 7304−7310.
(35) Schmickler, W.; Santos, E. *Interfacial Electrochemistry*, 2nd ed.; Springer: Berlin, 2010.
(36) Migliore, A.; Nitzan, A. Nonlinear Charge Transport in Redox Molecular Junctions: A Marcus Perspective. *ACS Nano* **2011**, *5*, 6669−6685.
(37) Schmickler, W. A Theory of Adiabatic Electron-Transfer Reactions. *J. Electroanal. Chem. Interfacial Electrochem.* **1986**, *204*, 31−43.
(38) Baldea, I. Important Insight into Electron Transfer in Single-Molecule Junctions Based on Redox Metalloproteins from Transition Voltage Spectroscopy. *J. Phys. Chem. C* **2013**, *117*, 25798−25804.
(39) Medvedev, I. G. Tunnel Current through a Redox Molecule Coupled to Classical Phonon Modes in the Strong Tunneling Limit. *Phys. Rev. B: Condens. Matter Mater. Phys.* **2007**, *76*, 125312.
(40) Baldea, I. Ambipolar Transition Voltage Spectroscopy: Analytical Results and Experimental Agreement. *Phys. Rev. B: Condens. Matter Mater. Phys.* **2012**, *85*, No. 035442.
(41) Kuznetsov, A.; Ulstrup, J. Mechanisms of in Situ Scanning Tunneling Microscopy of Organized Redox Molecular Assemblies. *J. Phys. Chem. A* **2000**, *104*, 11531−11540.
(42) Artés, J.; López-Martínez, M.; Giraudet, A.; Díez-Pérez, I.; Sanz, F.; Gorostiza, P. Current-Voltage Characteristics and Transition Voltage Spectroscopy of Individual Redox Proteins. *J. Am. Chem. Soc.* **2012**, *134*, 20218−20221.
(43) Landau, A.; Kronik, L.; Nitzan, A. Cooperative Effects in Molecular Conduction. *J. Comput. Theor. Nanosci.* **2008**, *5*, 535−544.
(44) Williams, P. D.; Reuter, M. G. Level Alignments and Coupling Strengths in Conductance Histograms: The Information Content of a Single Channel Peak. *J. Phys. Chem. C* **2013**, *117*, 5937−5942.
(45) Frisenda, R.; Perrin, M. L.; Valkenier, H.; Hummelen, J. C.; van der Zant, H. S. J. Statistical Analysis of Single-Molecule Breaking Traces. *Phys. Status Solidi B* **2013**, *250*, 2431−2436.
(46) Zhang, Y.; Liu, C.; Balaeff, A.; Skourtis, S. S.; Beratan, D. Biological Charge Transfer via Flickering Resonance. *Proc. Natl. Acad. Sci. U. S. A.* **2014**, *111*, 10049−10054.
(47) Cascella, M.; Magistrato, A.; Tavernelli, I.; Carloni, P.; Rothlisberger, U. Role of Protein Frame and Solvent for the Redox Properties of Azurin from *Pseudomonas aeruginosa*. *Proc. Natl. Acad. Sci. U. S. A.* **2006**, *103*, 19641−19646.
(48) Sigfridsson, E.; Olsson, M. H. M.; Ryde, U. A Comparison of the Inner-Sphere Reorganization Energies of Cytochromes, Iron-Sulfur Clusters, and Blue Copper Proteins. *J. Phys. Chem. B* **2001**, *105*, 5546−5552.
(49) Yuan, L.; Wang, L.; Garrigues, A. R.; Jiang, L.; Annadata, H. V.; Anguera Antonana, M.; Barco, E.; Nijhuis, C. A. Transition from Direct to Inverted Charge Transport Marcus Regions in Molecular Junctions via Molecular Orbital Gating. *Nat. Nanotechnol.* **2018**, *13*, 322−329.
(50) Fereiro, J.; Yu, X.; Pecht, I.; Sheves, M.; Cuevas, J. C.; Cahen, D. Tunneling Explains Efficient Electron Transport via Protein Junctions. *Proc. Natl. Acad. Sci. U. S. A.* **2018**, *115*, E4577−E4583.
(51) Livshits, G.; Stern, A.; Rotem, D.; Borovok, N.; Eidelshtein, G.; Migliore, A.; Penzo, E.; Wind, S.; Di Felice, R.; Skourtis, S. S.; et al. Long-Range Charge Transport in Single G-quadruplex DNA Molecules. *Nat. Nanotechnol.* **2014**, *9*, 1040−1046.
(52) Lehmann, L.; Ingold, G.-L.; Hanggi, P. Incoherent Charge Transport through Molecular Wires: Interplay of Coulomb Interaction and Wire Population. *Chem. Phys.* **2002**, *281*, 199−209.
(53) Milan-Garces, E.; Kaptan, S.; Puranik, M. Mode-Specific Reorganization Energies and Ultrafast Solvation Dynamics of Tryptophan from Raman Line-Shape Analysis. *Biophys. J.* **2013**, *105*, 211−221.
(54) Bard, A. J.; Faulkner, L. R. *Electrochemical Methods. Fundamentals and Applications*, 2nd ed.; John Wiley & Sons, Inc.: New York, 2000.
(55) Trasatti, S. The Absolute Electrode Potential: An Explanation Note. *Pure Appl. Chem.* **1986**, *58*, 955−966.
(56) Pascher, T.; Karlsson, B. G.; Nordling, M.; Malmstrom, B. G.; Vanngard, T. Reduction Potentials and Their pH Dependence in Site-Directed-Mutant Forms of Azurin from Pseudomas Aeruginosa. *Eur. J. Biochem.* **1993**, *212*, 289−296.
(57) Khoshtariya, D. E.; Dolidze, T. D.; Tretyakova, T.; Waldeck, D. H.; van Eldik, R. Electron Transfer with Azurin at Au-SAM Junctions in Contact with a Protic Ionic Melt: Impact of Glassy Dynamics. *Phys. Chem. Chem. Phys.* **2013**, *15*, 16515−16526.
(58) Matelkova, K.; Ossberger, K.; Hudak, J.; Vatral, J.; Boca, R.; Linert, W. Redox activity of some non-innocent amino acids. *Monatsh. Chem.* **2013**, *144*, 937−949.
(59) Sachtler, W. M. H.; Dorgelo, G. J. H.; Holscher, A. A. The work function of gold. *Surf. Sci.* **1966**, *5*, 221−229.
(60) Troisi, A.; Nitzan, A.; Ratner, M. A. A Rate Constant Expression for Charge Transfer through Fluctuating Bridges. *J. Chem. Phys.* **2003**, *119*, 5782−5788.
(61) Migliore, A.; Nitzan, A. Irreversibility and Hysteresis in Redox Molecular Conduction Junctions. *J. Am. Chem. Soc.* **2013**, *135*, 9420−9432.
(62) White, A. J.; Migliore, A.; Galperin, M.; Nitzan, A. Quantum Transport with Two Interacting Conduction Channels. *J. Chem. Phys.* **2013**, *138*, 174111.

DOI: 10.1021/acs.jpcc.9b00135
J. Phys. Chem. C 2019, 123, 5907−5922